Journal of Sound and Vibration (2002) **256**(4), 695–724
doi:10.1006/jsvi.5017, available online at http://www.idealibrary.com on IDEAL®

EXPLICIT PREDICTOR–MULTICORRECTOR TIME DISCONTINUOUS GALERKIN METHODS FOR NON-LINEAR DYNAMICS

A. Bonelli and O. S. Bursi

Dipartimento di Ingegneria Meccanica e Strutturale, Università di Trento, Via Mesiano 77, 38050 *Trento, Italy. E-mail: alessio.bonelli@ing.unitn.it*

and

M. Mancuso

Dipartimento di Scienze dell'Ingegneria, Università di Modena e Reggio Emilia, 41100 *Modena, Italy*

(*Received* 21 *September* 2001, *and in final form* 21 *January* 2002)

Explicit predictor–multicorrector time discontinuous Galerkin (TDG) methods developed for linear structural dynamics are formulated and implemented in a form suitable for arbitrary non-linear analysis of structural dynamics problems. The formulation is intended to inherit the accuracy properties of the exact parent implicit TDG methods. To this end, suitable predictors and correctors are designed to achieve third order accuracy, large stability limits and controllable numerical dissipation by means of an algorithmic parameter. As the study of a general non-linear case is rather complex, the analysis of the convergence properties of the resulting algorithms are restricted to conservative Duffing oscillators, for which closed-form solutions are available. It is shown that the main properties of the underlying parent scheme can be retained. Finally, results of representative numerical simulations relevant to Duffing oscillators and to a stiff spring pendulum discretized with finite elements illustrate the performance of the numerical schemes and confirm the analytical estimates.

1. INTRODUCTION

The numerical solution of problems in structural dynamics requires the time integration of a system of ordinary differential equations. Finite difference-based time-stepping schemes are widely used tools [1, p. 490]; however, particular attention is required for application to non-linear problems, as these schemes were mainly developed in the context of linear problems. For instance, the trapezoidal rule which is unconditionally stable (A-stable) and non-dissipative in the linear case, does not guarantee a stable time integration in the non-linear case. This drawback has been reported in several studies and much research has been devoted to the development of more robust implicit algorithms for non-linear dynamics (see references [2, p. 447, references therein; 3] among others). With regard to explicit algorithms, the second order central difference (CD) method is still the most popular explicit scheme [1, p. 495]. Nonetheless, several explicit schemes devoted to linear and non-linear problems have been proposed recently. For instance, Chung and Lee [4] developed an explicit scheme with controllable high-frequency dissipation for linear and non-linear structural dynamics. Macek and Aubert [5] proposed a modified central

0022-460X/02/$35.00

difference scheme with a mass penalty technique able to lower the highest natural frequency of the dynamical system under examination. Other applications of finite difference schemes can be found in reference [6], with reference to Burger's non-linear one-dimensional equation. Both accuracy and stability properties have been checked in the linear case for this scheme, while the convergence properties have been proved in the non-linear regime by numerical simulation only.

Questions related to how explicit schemes perform on non-linear systems, particularly when non-linearity is an issue, are still a matter of investigation. Examples are the papers by Hoff and Taylor [7, 8], in which a high order explicit method has been analyzed both in the linear and non-linear regimes. In the case of strong non-linearities, it has been demonstrated that the scheme may decrease its order of accuracy to two; in addition, it has been proved that the scheme may exhibit unstable behaviour owing to sudden stiffening or large displacement increments.

Another factor which could impair performance of an explicit algorithm applied to non-linear cases, is non-physical oscillation, related to spurious high-frequency modes introduced by spatial discretization [1, p. 498]. In fact, the CD scheme does not introduce any algorithmic damping; thereby inaccurate results owing to the integration of spurious modes, artefact of modelling, may be obtained. To avoid such unexpected effects, algorithmic dissipation in the high-frequency modes should be introduced. See, for instance, the explicit HCE-α method of Hulbert and Chung [9], designed purposely to annihilate high-frequency oscillation modes.

An alternative approach to numerical time integration of structural systems is based on Galerkin formulations in the time domain [10–13]. In such schemes, the space is discretized using conventional finite elements, the time interval is partitioned in a number of subintervals, while the response is approximated by means of trial functions in the time variable. The use of discontinuous displacement and momentum fields leads to the class of implicit schemes, named time discontinuous Galerkin (TDG) methods. These unconditionally stable schemes damp out any undesirable high-frequency mode, without introducing excessive algorithmic damping in the low-frequency response. Nonetheless, the factorization of a matrix larger than the one exploited in standard implicit schemes is required owing to unknown extra displacement and momentum fields. In order to limit the computational effort, Li and Wiberg [14] implemented a predictor–multicorrector solution algorithm in the TDG method. Such an algorithm requires the factorization of a reduced matrix for each fixed time-step size, and few iterations for solving the resulting system of coupled equations in the unknown velocities. The same authors also proposed TDG methods based on an explicit time integration [15, 16]. The resulting explicit scheme was third order accurate and endowed with a stability limit higher than that of the CD method. Third order accuracy was also proved for a non-linear Duffing oscillator, while the stability limit estimated for the linear case was employed in the non-linear case too.

Based on similar strategies, a new class of explicit TDG methods, with a user-defined dissipation, has been developed by Bonelli *et al.* [17]. The new proposed schemes, designated E schemes, have been implemented in a predictor–multicorrector form, exhibit third order accuracy and accrue a stability limit higher than the one of the CD scheme. However, the convergence and dissipation properties of such algorithms are not so obvious in the non-linear case. In fact, the limited number of correctors combined to severe non-linearities may impair their favourable properties. Therefore, the E schemes are analyzed in this paper to evaluate both their convergence properties and their extension to the non-linear case.

The analysis of a general non-linear case is rather complex mainly due to the strong link between the scheme performance and the type of non-linearity. A common approach in

structural dynamics entails the convergence analysis on relatively simple non-linear test problems [18, p. 424; 19–23], which can describe cases of interest. This procedure has also been chosen in this paper and therefore, the accuracy and stability analysis of the E schemes is restricted to conservative Duffing oscillators. These single-degree-of-freedom (s.d.o.f.) systems are representative of a large class of strong non-linear hardening and softening structural problems [18, p. 424], and are often assumed as test problems for the evaluation of time-stepping schemes [15, 21, 22, p. 245].

In view of arbitrary non-linear analysis, the time integration of a stiff ordinary differential equation representative of a system discretized in space with finite elements is also considered [23, p. 9, 24]. Therefore, several simulations are performed on a stiff spring pendulum, which exhibits a large and relatively slow circular motion coupled to a high-frequency axial motion, artefact of the modelling [3]. In order to limit the influence of the high-frequency internal motion on the global physical solution, the E schemes must dissipate the axial motion and conserve the circular motion in the medium to long term. To a lesser extent, simulation is also performed with finite difference-based schemes, like the CD and the HCE-α methods.

The remainder of the paper is organized as follows. In section 2, a formulation of the TDG method is presented. Section 3.1 is devoted to the formulation of the explicit E methods in the non-linear regime, while the implementation characteristics of the E schemes are drawn in section 3.2. Section 4 illustrates the convergence analyses of the schemes applied to the non-linear Duffing oscillator model problems. Section 5 presents numerical simulations which illustrate the performance of the methods as predicted from theoretical analysis, while concluding remarks are reported in section 6.

2. FORMULATION OF THE IMPLICIT TDG METHOD

The semidiscrete initial value problem with the initial conditions reads

$$\begin{aligned} &\mathbf{M}\ddot{\mathbf{q}}(t) + \mathbf{C}\dot{\mathbf{q}}(t) + \mathbf{S}(\mathbf{q}(t)) = \mathbf{f}(t), \quad t \in I = (0, t_N), \\ &\mathbf{q}(0) = \bar{\mathbf{q}}_0, \\ &\dot{\mathbf{q}}(0) = \bar{\mathbf{v}}_0. \end{aligned} \tag{1}$$

where the state variables $\mathbf{q}(t)$ and $\dot{\mathbf{q}}(t)$ are the nodal quantities arising from the spatial discretization. To obtain equation (1_1) a standard finite element-based discretization [1] is used. Note that the subscript of equation (1_1) points out the first equation in system (1). Let $\mathbf{M}$ denote the symmetric positive-definite mass matrix, $\mathbf{C}$ the viscous damping matrix, $\mathbf{S}(\mathbf{q}(t))$ the vector of non-linear internal forces, $\mathbf{f}(t)$ the vector of applied forces and I the time domain. The superposed dots indicate differentiation with respect to time t. $\bar{\mathbf{q}}_0$ and $\bar{\mathbf{v}}_0$ are the prescribed initial displacement and velocity vectors. The initial value problem (1) can be rewritten in the first order form

$$\begin{aligned} &\dot{\mathbf{p}}(t) + \mathbf{C}\mathbf{M}^{-1}\mathbf{p}(t) + \mathbf{S}(\mathbf{q}(t)) = \mathbf{f}(t), \quad t \in I = (0, t_N), \\ &\mathbf{M}^{-1}\mathbf{p}(t) - \dot{\mathbf{q}}(t) = \mathbf{0}, \quad t \in I = (0, t_N), \\ &\mathbf{q}(0) = \bar{\mathbf{q}}_0, \\ &\mathbf{p}(0) = \bar{\mathbf{p}}_0 = \mathbf{M}\bar{\mathbf{v}}_0, \end{aligned} \tag{2}$$

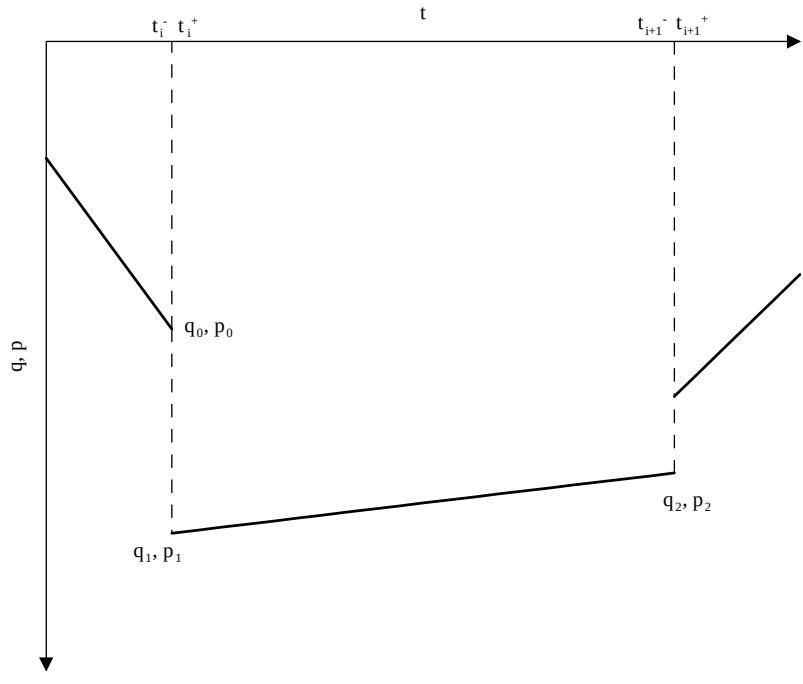

Figure 1. Time finite elements with linear test and weight functions.

where $\mathbf{q}(t)$ and $\mathbf{p}(t)$ denote the generalized displacement and momentum vector. The standard TDG methods are one-step methods derived from Galerkin weighted residual formulations of equations (2), with the initial conditions imposed in a weak manner at each time step. Hereinafter, a two-field formulation is considered with displacement and momentum as independent fields. Moreover, attention is restricted to the method obtained using linear time interpolants. In such conditions, third order accuracy and L stability can be achieved in linear regime, namely, high-frequency modes are damped out nearly in one time step [12]. Consider a partition of the time domain

$$I_i = (t_i, t_{i+1}), \quad i = 0, \ldots, N, \tag{3}$$

where $0 = t_0 < t_1 < \cdots < t_i < t_{i+1} < \cdots < t_N$ and $\Delta t = t_{i+1} - t_i$ is the time-step size. Let $(\mathbf{q}_0, \mathbf{p}_0)$ denote the vectors of displacement and momentum at $t_i^- = \lim_{t \to t_i^-} t$, which are known from either the previous step calculation or the initial data ($\bar{\mathbf{q}}_0$ and $\bar{\mathbf{p}}_0$) if $i = 0$. Moreover, let $(\mathbf{q}_1, \mathbf{p}_1)$ and $(q_2, \mathbf{p}_2)$ denote the displacement and momentum at $t_i^+ = \lim_{t \to t_i^+} t$ and t_{i+1}^-, respectively, which represent the four unknown vectors in the time interval (t_i^+, t_{i+1}^-) . Such quantities are illustrated schematically in Figure 1. Displacement and momentum at an arbitrary time $t \in (t_i,\ t_{i+1})$ are expressed as

$$\begin{aligned} \mathbf{q}(t) &= t_1(t)\ \mathbf{q}_1 + t_2(t)\ \mathbf{q}_2, \\ \mathbf{p}(t) &= t_1(t)\ \mathbf{p}_1 + t_2(t)\ \mathbf{p}_2, \end{aligned} \tag{4}$$

where the interpolation polynomials read

$$t_1(t) = \frac{(t_{i+1} - t)_i}{\Delta t}, \qquad t_2(t) = \frac{(t - t_i)}{\Delta t}. \tag{5}$$

The corresponding weighting functions are chosen as

$$\mathbf{w}_{\mathbf{q}}(t) = t_1(t)\mathbf{w}_{\mathbf{q}_1} + t_2(t)\mathbf{w}_{\mathbf{q}_2},$$
$$\mathbf{w}_{\mathbf{p}}(t) = t_1(t)\mathbf{w}_{\mathbf{p}_1} + t_2(t)\mathbf{w}_{\mathbf{p}_2}. \tag{6}$$

With this notation to hand, the TDG1 method is obtained enforcing the weighted residual form of equations (2): find $(\mathbf{q}_1, \mathbf{p}_1)$ and $(\mathbf{q}_2, \mathbf{p}_2)$ such that

$$\begin{aligned}\int_{I_i} w_{\mathbf{q}}^{\mathrm{T}}(\dot{\mathbf{p}}(t) + \mathbf{C}\mathbf{M}^{-1}\mathbf{p}(t) + \mathbf{S}(\mathbf{q}(t)) - \mathbf{f}(t))\,\mathrm{d}t \\ + \int_{I_i} \mathbf{w}_{\mathbf{p}}^{\mathrm{T}}(t)(\mathbf{M}^{-1}\mathbf{p}(t) - \dot{\mathbf{q}}(t))\,\mathrm{d}t \\ - \mathbf{w}_{\mathbf{p}}^{\mathrm{T}}(t_i^+)(\mathbf{q}(t_i^+) - \mathbf{q}_0) \\ + \mathbf{w}_{\mathbf{q}}^{\mathrm{T}}(t_i^+)(\mathbf{p}(t_i^+) - \mathbf{p}_0) = 0\end{aligned} \tag{7}$$

for all $\mathbf{w}_{\mathbf{q}_1}, \mathbf{w}_{\mathbf{q}_2}, \mathbf{w}_{\mathbf{p}_1}, \mathbf{w}_{\mathbf{p}_2}$. Note that the initial conditions are weakly enforced in equation (7) and, as such, the numerical solution can be discontinuous between time steps; hence the denomination of TDG1 algorithm. Such discontinuity is depicted in Figure 1 and systematically leads to energy-decaying schemes, i.e., schemes eliminating the energy associated with vibratory motion at high frequency [14]. Substituting equations (4) and (6) into equation (7), the following algebraic system is obtained:

$$\begin{aligned}\mathbf{P}_{\mathbf{q}1} + \left(\frac{1}{2}\mathbf{I} + \frac{\Delta t}{3}\mathbf{C}\mathbf{M}^{-1}\right)\mathbf{p}_1 + \left(\frac{1}{2}\mathbf{I} + \frac{\Delta t}{6}\mathbf{C}\mathbf{M}^{-1}\right)\mathbf{p}_2 = \mathbf{p}_0 + \mathbf{F}_1, \\ \mathbf{P}_{\mathbf{q}2} + \left(-\frac{1}{2}\mathbf{I} + \frac{\Delta t}{6}\mathbf{C}\mathbf{M}^{-1}\right)\mathbf{p}_1 + \left(\frac{1}{2}\mathbf{I} + \frac{\Delta t}{3}\mathbf{C}\mathbf{M}^{-1}\right)\mathbf{p}_2 = \mathbf{F}_2, \\ -\frac{1}{2}\mathbf{q}_1 - \frac{1}{2}\mathbf{q}_2 + \frac{\Delta t}{3}\mathbf{M}^{-1}\mathbf{p}_1 + \frac{\Delta t}{6}\mathbf{M}^{-1}\mathbf{p}_2 = -\mathbf{q}_0, \\ \frac{1}{2}\mathbf{q}_1 - \frac{1}{2}\mathbf{q}_2 + \frac{\Delta t}{6}\mathbf{M}^{-1}\mathbf{p}_1 + \frac{\Delta t}{3}\mathbf{M}^{-1}\mathbf{p}_2 = 0,\end{aligned} \tag{8}$$

where

$$\begin{aligned}\mathbf{P}_{\mathbf{q}1} = \int_{t_i}^{t_i+1} t_1(t)\,\mathbf{S}(t_1(t)\,\mathbf{q}_1 + t_2(t)\,\mathbf{q}_2)\,\mathrm{d}t, \\ \mathbf{P}_{\mathbf{q}2} = \int_{t_i}^{t_i+1} t_2(t)\,\mathbf{S}(t_1(t)\,\mathbf{q}_1 + t_2(t)\,\mathbf{q}_2)\,\mathrm{d}t \\ \mathbf{F}_1 = \int_{t_i}^{t_i+1} t_1(t)\,\mathbf{f}(t)\,\mathrm{d}t, \qquad \mathbf{F}_2 = \int_{t_i}^{t_i+1} t_2(t)\,\mathbf{f}(t)\,\mathrm{d}t.\end{aligned} \tag{9}$$

A drawback of the TDG1 method is related to the size of system (8), which is equal to $4n_{d.o.f.}$, where $n_{d.o.f.}$ is the number of degrees of freedom in the spatial discretization. This system is four times larger than the conventional time discretization of equation (1). Moreover, the global matrix is non-symmetrical.

To limit these drawbacks, we propose an explicit formulation derived directly from the implicit parent TDG1 method and implemented in an explicit predictor–multicorrector form with one and two corrector passes. The formulation represents an extension to the non-linear case of the explicit methods suggested in reference [17]. Therefore, an accuracy and stability analysis of these schemes is needed for the non-linear case. Clearly, the convergence properties of the parent implicit TDG method in the non-linear case depend on the integration rules employed in equation (9). Nonetheless, the effect of internal and external force approximations on the convergence of the schemes is not the object of this paper, and therefore, an exact integration is considered for the Duffing oscillators. For the more complicated problem, namely, the stiff spring pendulum, three-point Gauss–Legendre quadrature is exploited.

3. THE EXPLICIT PREDICTOR–MULTICORRECTOR METHODS

3.1. FORMULATION

For simplicity, the undamped ($\mathbf{C} = \mathbf{0}$) case is considered. The algorithms are derived from the implicit parent TDG1 scheme described in section (2), with the aim to retain both third order accuracy and favourable dissipative properties. In order to reduce the computational effort related to the solution of system (8) the explicit formulation relies on an iterative predictor–multicorrector procedure, where the number of correctors is limited to one or two. To this end, the unknown momenta $\mathbf{p}_1$ and $\mathbf{p}_2$ are eliminated from equations (8_3, 8_4), thus obtaining

$$\mathbf{x}_\mathbf{p} = \begin{bmatrix} \mathbf{p}_1 \\ \mathbf{p}_2 \end{bmatrix} = \begin{bmatrix} \dfrac{1}{\Delta t}\mathbf{M}(3\mathbf{q}_1 + \mathbf{q}_2 - 4\mathbf{q}_0) \\ \dfrac{1}{\Delta t}\mathbf{M}(-3\mathbf{q}_1 + \mathbf{q}_2 + 2\mathbf{q}_0) \end{bmatrix}. \tag{10}$$

Substituting equation (10) into the equations (8_1, 8_2) and multiplying the second equation by $-\frac{1}{3}$, the following system is obtained:

$$\mathbf{B}\,\mathbf{x}_\mathbf{q} + \mathbf{P}_\mathbf{q} - \mathbf{P}_0 = 0, \tag{11}$$

where

$$\mathbf{B} = \frac{1}{\Delta t}\begin{bmatrix} \mathbf{0} & \mathbf{M} \\ \mathbf{M} & \mathbf{0} \end{bmatrix}, \qquad \mathbf{x}_\mathbf{q} = \begin{bmatrix} \mathbf{q}_1 \\ \mathbf{q}_2 \end{bmatrix},$$

$$\mathbf{P}_0 = \begin{bmatrix} \mathbf{p}_0 + \dfrac{1}{\Delta t}\mathbf{M}q_0 + \mathbf{F}_1 \\ \dfrac{1}{\Delta t}\mathbf{M}q_0 - \dfrac{1}{3}\mathbf{F}_2 \end{bmatrix}, \qquad \mathbf{P}_\mathbf{q} = \begin{bmatrix} \mathbf{P}_{q_1} \\ -\frac{1}{3}\mathbf{P}_{q_2} \end{bmatrix}. \tag{12}$$

System (11) is solved in terms of the unknown displacement vector $\mathbf{x}_q$. In fact, a formulation in the unknown momenta has also been suggested in reference [16]. Nonetheless, as the non-linear reaction forces depend mainly on displacements, see equation (1), the displacement vector $\mathbf{x}_\mathbf{q}$ has necessarily to be evaluated to estimate the vector $\mathbf{P}_\mathbf{q}$. Moreover,

the vector $\mathbf{p}_1$ defined in equation (10_1) is not used and therefore, the computational effort is limited avoiding one vector storage.

Let $\mathbf{x}_{\mathbf{q}}^{(k)}$ denote the kth trial value of the unknown displacement vector in a typical time step $[t_i, t_{i+1}]$. In order to advance from t_i to t_{i+1}, the following steps are performed.

3.1.1. *Predictor*

The predictor relies on the Taylor series expansion of the solution of the implicit parent TDG1 algorithm

$$\begin{aligned} \mathbf{q}_1 &= \mathbf{q}_0 - \frac{\Delta t^2}{6}\mathbf{M}^{-1}\dot{\mathbf{p}}_0 + \mathbf{O}(\Delta t^3), \\ \mathbf{q}_2 &= \mathbf{q}_0 + \Delta t\mathbf{M}^{-1}\mathbf{p}_0 + \frac{\Delta t^2}{2}\mathbf{M}^{-1}\dot{\mathbf{p}}_0 + \mathbf{O}(\Delta t^3). \end{aligned} \tag{13}$$

where $\dot{\mathbf{p}}_0$ defines the time derivative of momentum evaluated at t_i^- according to Figure 1; it can be obtained from the equilibrium equation (2), namely,

$$\dot{\mathbf{p}}_0 = f(t_0) - \mathbf{S}(\mathbf{q}_0). \tag{14}$$

In order to achieve optimal accuracy and dissipative properties, $\mathbf{x}_{\mathbf{q}}$ is expressed in terms of free parameters a and b

$$\mathbf{x}_{\mathbf{q}}^{(0)} = \begin{bmatrix} \mathbf{q}_1^{(0)} \\ \mathbf{q}_2^{(0)} \end{bmatrix} = \begin{bmatrix} \mathbf{q}_0 + a\Delta t^2\mathbf{M}^{-1}\dot{\mathbf{p}}_0 \\ \mathbf{q}_0 + \Delta t\mathbf{M}^{-1}\mathbf{p}_0 + b\Delta t^2\mathbf{M}^{-1}\dot{\mathbf{p}}_0 \end{bmatrix}, \tag{15}$$

where $k = 0$ is used to initialize the unknowns.

3.1.2 *Corrector*

In order to obtain approximate solutions of system (11), an iterative scheme based on displacement increments is exploited. More specifically, it suffices to define the residual

$$\mathbf{r}^{(k)} = \mathbf{B}\,\mathbf{x}_{\mathbf{q}}^{(k)} + \mathbf{P}_{\mathbf{q}}^{(k)} - \mathbf{P}_0 \tag{16}$$

and the displacement increment

$$\Delta\mathbf{x}_{\mathbf{q}}^{(k)} = -\mathbf{B}^{-1}\mathbf{r}^{(k)}. \tag{17}$$

The new class of schemes exploiting predictor (15) with a limited number k_{max} of correctors is the extension to the non-linear case of the schemes proposed in reference [17] for the linear case. The schemes are denoted E methods and, more specifically, E-1C defines the scheme requiring one corrector pass ($k_{max} = 1$) while the acronym E-2C stands for the method adopting two corrector passes ($k_{max} = 2$).

3.2. IMPLEMENTATION

The solution procedure of the E methods applied to non-linear problems is as follows:

1. Initial computations:
   (a) Form the diagonal mass matrix $\mathbf{M}$.
   (b) Initialize $\bar{\mathbf{q}}_0$, $\bar{\mathbf{p}}_0$, $\mathbf{S}(\bar{\mathbf{q}}_0)$ and $\mathbf{f}(t_0)$.
   (c) Select the number of correctors k_{max} (1 or 2), the value of the parameters a and b as well as the time-step size Δt

2. For each time step ($i = 0, 1, \ldots, N$),

(a) Compute the momenta time derivative at time t_i^-

$$\dot{\mathbf{p}}_i = \mathbf{f}(t_i) - \mathbf{S}(\mathbf{q}_i).$$

(b) Compute the vectors $\mathbf{P}_{i,1}$ and $\mathbf{P}_{i,2}$ based on initial conditions and external force (equations 12_3, 12_4))

$$\mathbf{P}_{i,1} = \mathbf{p}_i + \frac{1}{\Delta t}\mathbf{M}\mathbf{q}_i + \int_{t_i}^{t_i+1} t_1(t)\,\mathbf{f}(t_i + t)\,\mathrm{d}t,$$

$$\mathbf{P}_{i,2} = \frac{1}{\Delta t}\mathbf{M}\mathbf{q}_i - \frac{1}{3}\int_{t_i}^{t_i+1} t_2(t)\,\mathbf{f}(t_i + t)\,\mathrm{d}t.$$

(c) Compute the predictor displacements (equation (15)) at time t_i^+ and t_{i+1}^-, respectively,

$$\mathbf{q}_1^{(0)} = \mathbf{q}_i + a\,\Delta t^2\,\mathbf{M}^{-1}\dot{\mathbf{p}}_i,$$

$$\mathbf{q}_2^{(0)} = \mathbf{q}_i + \Delta t\mathbf{M}^{-1}\mathbf{p}_i + b\Delta t^2\mathbf{M}^{-1}\dot{\mathbf{p}}_i.$$

(d) Set $k = 0$.

(e) Multicorrector:

(i) Compute the integrals of internal force vector $\mathbf{S}(\mathbf{q})$

$$\mathbf{P}_{\mathbf{q}1}^{(k)} = \int_{t_i}^{t_i+1} t_1(t)\,\mathbf{S}(t_1(t)\mathbf{q}_1^{(k)} + t_2(t)\mathbf{q}_2^{(k)})\,\mathrm{d}t,$$

$$\mathbf{P}_{q2}^{(k)} = \int_{t_i}^{t_i+1} t_2(t)\,\mathbf{S}(t_1(t)\mathbf{q}_1^{(k)} + t_2(t)\mathbf{q}_2^{(k)})\,\mathrm{d}t.$$

(ii) Compute the residual vectors (equation (16))

$$r_1^{(k)} = \frac{1}{\Delta t}\mathbf{M}\mathbf{q}_2^{(k)} + \mathbf{P}_{\mathbf{q}1}^{(k)} - \mathbf{P}_{i,1},$$

$$\mathbf{r}_2^{(k)} = \frac{1}{\Delta t}\mathbf{M}\mathbf{q}_1^{(k)} - \frac{1}{3}\mathbf{P}_{\mathbf{q}2}^{(k)} - \mathbf{P}_{i,2}.$$

(iii) Compute the displacement increments (equation (17))

$$\Delta\mathbf{q}_1 = \Delta t\mathbf{M}^{-1}\mathbf{r}_2,$$

$$\Delta\mathbf{q}_2 = \Delta t\,\mathbf{M}^{-1}\mathbf{r}_1.$$

(iv) Compute the displacement vectors

$$\mathbf{q}_1^{(k+1)} = \mathbf{q}_1^{(k)} + \Delta\mathbf{q}_1,$$

$$\mathbf{q}_2^{(k+1)} = \mathbf{q}_2^{(k)} + \Delta\mathbf{q}_2.$$

(v) $k = k + 1$

(vi) If $k < k_{max}$ go to 2(e)(i).

(f) Compute the displacement vector at time $t_{i+1} = t_i + \Delta t$

$$\mathbf{q}_{i+1} = \mathbf{q}_2^{(k)}.$$

(g) Compute the momentum vector at time $t_{i+1} = t_i + \Delta t$ (equation (10))

$$\mathbf{p}_{i+1} = \frac{1}{\Delta t}\mathbf{M}(-3\mathbf{q}_1^{(k)} + \mathbf{q}_2^{(k)} + 2\mathbf{q}_i).$$

(h) $i = i + 1$.

(i) If $i < N$ go to 2(a).

The parameters a and b are selected to achieve third order accuracy and controllable dissipative properties. Such issues are treated thoroughly in section 4. Moreover, differently from the explicit formulation suggested in reference [15], the proposed schemes avoid the evaluation of $\mathbf{p}_1$ in each iteration and compute $\mathbf{p}_{i+1}$ only at the iteration end.

4. ACCURACY AND STABILITY ANALYSIS

In this section, it is demonstrated that the predictor–multicorrector algorithms described in section 3 can substantially retain the properties of the E methods developed for linear systems [17]. It is well known that a scheme designed for linear dynamics can be analyzed by considering a simple model problem which describes the time evolution of a generic vibration mode [1, p. 492]. Nonetheless, the standard modal decomposition procedure cannot be applied to equations (2). Therefore, non-linear test problems exhibiting key features typical of more complex systems arising in non-linear dynamics are chosen: namely, unforced and undamped Duffing oscillators [25, 22, p. 245]. Such oscillators are described by means of equation (42) and are discussed at length in section 5.1.

4.1. ITERATION MATRIX

In a s.d.o.f. problem the matrices in equation (1) become scalar and the vector $\mathbf{x}_\mathbf{q}$ in equation $(12)_2$ collects only two components. Defining a secant stiffness operator $\mathbf{D}$ which satisfies the equation

$$\mathbf{P}_\mathbf{q}^{(k)} = \mathbf{D}(x_\mathbf{q}^{(k)})\mathbf{x}_\mathbf{q}^{(k)} \tag{18}$$

and combining equations (16) and (17), a relation between two iterations can be found. More specifically, such relation reads

$$\begin{aligned}\mathbf{x}_\mathbf{q}^{(k+1)} = \mathbf{x}_\mathbf{q}^{(k)} + \Delta\mathbf{x}_\mathbf{q}^{(k+1)} &= \mathbf{x}_\mathbf{q}^{(k)} - \mathbf{B}^{-1}r^{(k)}(\mathbf{x}_\mathbf{q}^{(k)}) = \mathbf{x}_\mathbf{q}^{(k)} - \mathbf{B}^{-1}(\mathbf{B}x_\mathbf{q}^{(k)} + \mathbf{P}_\mathbf{q}^{(k)} - \mathbf{P}_0)\\ &= [\mathbf{I} - \mathbf{B}^{-1}(\mathbf{B} + \mathbf{D}(\mathbf{x}_\mathbf{q}^{(k)}))]\mathbf{x}_\mathbf{q}^{(k)} + \mathbf{B}^{-1}\mathbf{P}_0 = -\mathbf{B}^{-1}\mathbf{D}(\mathbf{x}_\mathbf{q}^{(k)})\mathbf{x}_\mathbf{q}^{(k)} + \mathbf{B}^{-1}\mathbf{P}_0\end{aligned} \tag{19}$$

and can be expressed in the form

$$\mathbf{x}_\mathbf{q}^{(k+1)} = \mathbf{A}_{IT}(\mathbf{x}_\mathbf{q}^{(k)})\, x_\mathbf{q}^{(k)} + \mathbf{g}, \tag{20}$$

where the iteration matrix $\mathbf{A}_{IT}(\mathbf{x}_{\mathbf{q}}^{(k)}) = -\mathbf{B}^{-1}\mathbf{D}(\mathbf{x}_{\mathbf{q}}^{(k)})$ while $\mathbf{g} = \mathbf{B}^{-1}\mathbf{P}_0$ takes into account both initial conditions and external forces. Assuming for simplicity $M = 1$ in equation (42), $\mathbf{A}_{IT}$ and $\mathbf{g}$ read

$$\mathbf{A}_{IT}(\mathbf{x}_{\mathbf{q}}^{(k)}) = \begin{bmatrix} \dfrac{\Delta t^2 S_1 (10 + 3 S_2 (q_1^{(k)})^2 + 9 S_2 (q_2^{(k)})^2)}{180} & \dfrac{\Delta t^2 S_1 (10 + 3 S_2 (q_1^{(k)})^2 + 6 S_2 (q_2^{(k)})^2)}{90} \\ -\dfrac{\Delta t^2 S_1 (10 + 6 S_2 (q_1^{(k)})^2 + 3 S_2 (q_2^{(k)})^2)}{30} & -\dfrac{\Delta t^2 S_1 (10 + 9 S_2 (q_1^{(k)})^2 + 3 S_2 (q_2^{(k)})^2)}{60} \end{bmatrix} \tag{21}$$

and

$$\mathbf{g} = \begin{bmatrix} q_0 \\ \Delta t\, p_0 + \mathbf{q}_0 \end{bmatrix} \tag{22}$$

respectively.

4.2. TIME-ADVANCE SCHEME

Both the consistency and stability analysis are based on the following time-advance scheme:

$$\mathbf{y}_1 = \mathscr{A}(\mathbf{y}_0, S_1, S_2, \Delta t), \tag{23}$$

where, recalling the notation employed in Figure 1,

$$\mathbf{y}_0 = \begin{bmatrix} q_0 \\ p_0 \end{bmatrix} \quad \text{and} \quad \mathbf{y}_1 = \begin{bmatrix} q_2 \\ p_2 \end{bmatrix}. \tag{24}$$

The analytic expression of equation (23) can be readily obtained as the schemes are explicit. Equation (23) depends on equations (15) and (20), as such, $\mathbf{x}_{\mathbf{q}}^{(0)}$ $\mathbf{A}_{IT}$ and $\mathbf{g}$ can be exploited. More specifically, assuming again $M = 1$ the predictor reads

$$\mathbf{x}_{\mathbf{q}}^{(0)} = \begin{bmatrix} q_1^{(0)} \\ q_2^{(0)} \end{bmatrix} = \mathbf{E}\mathbf{y}_0, \tag{25}$$

where the matrix $\mathbf{E}$

$$\mathbf{E} = \begin{bmatrix} 1 - \Delta t^2 a S_1 (1 + S_2 q_0^{2)} & 0 \\ 1 - \Delta t^2 b S_1 (1 + S_2 q_0^{2)} & \Delta t \end{bmatrix} \tag{26}$$

relies on free parameters a and b and provides an initial guess for equation (20). The vector $\mathbf{g}$ reads

$$\mathbf{g} = \mathbf{G}\mathbf{y}_0, \tag{27}$$

where

$$\mathbf{G} = \begin{bmatrix} 1 & 1 \\ 0 & \Delta t \end{bmatrix}, \tag{28}$$

and depends on the initial conditions only. As a result, the unknown displacement vector $\mathbf{x_q}$ can be estimated performing k_{max} (1 or 2) correctors. Employing the iteration matrix $\mathbf{A}_{IT}$, it can be readily shown that

$$\mathbf{x_q} = \mathbf{x_q}^{(k_{max})} = \left(\prod_{i=1}^{k_{max}} \mathbf{A}_{IT}(\mathbf{x_q}^{(i-1)})\right)\mathbf{x_q}^{(0)} + \sum_{i=0}^{k_{max}-1}\left(\prod_{j=1}^{i} \mathbf{A}_{IT}(\mathbf{x_q}^{(j-1)})\right)\mathbf{g}$$

$$= \left(\prod_{i=1}^{k_{max}} \mathbf{A}_{IT}(\mathbf{x_q}^{(i-1)})\right)\mathbf{E}\mathbf{y}_0 + \sum_{i=0}^{k_{max}-1}\left(\prod_{j=1}^{i} \mathbf{A}_{IT}(\mathbf{x_q}^{(j-1)})\right)\mathbf{G}\mathbf{y}_0 = \mathbf{Q}\mathbf{y}_0, \tag{29}$$

where

$$\mathbf{Q} = \left[\left(\prod_{i=1}^{k_{max}} \mathbf{A}_{IT}(\mathbf{x_q}^{(i-1)})\right)\mathbf{E} + \sum_{i=0}^{k_{max}-1}\left(\prod_{j=1}^{i} \mathbf{A}_{IT}(\mathbf{x_q}^{(j-1)})\right)\mathbf{G}\right]. \tag{30}$$

Once $\mathbf{x_q}$ is determined, the momentum p_2 at the end of the time step can be evaluated from equation (10_2):

$$p_2 = -\frac{3}{\Delta t}q_1 + \frac{1}{\Delta t}q_2 + \frac{2}{\Delta t}q_0$$

$$= \mathbf{W}_1\mathbf{y}_0 + \mathbf{W}_2\mathbf{x}_q = (\mathbf{W}_1 + \mathbf{W}_2\mathbf{Q})\mathbf{y}_0, \tag{31}$$

where

$$\mathbf{W}_1 = \begin{bmatrix} \frac{2}{\Delta t} & 0 \end{bmatrix} \quad \text{and} \quad \mathbf{W}_2 = \begin{bmatrix} -\frac{3}{\Delta t} & \frac{1}{\Delta t} \end{bmatrix}. \tag{32}$$

Finally, the time-advance scheme reads

$$\mathbf{y}_1 = \mathscr{A}(\mathbf{y}_0, S_1, S_2, \Delta t) = \left(\begin{bmatrix} 0 & 1 \\ 0 & 0 \end{bmatrix}\mathbf{Q} + \begin{bmatrix} 0 \\ 1 \end{bmatrix}(\mathbf{W}_1 + \mathbf{W}_2\mathbf{Q})\right)\mathbf{y}_0. \tag{33}$$

4.3. CONSISTENCY

The local truncation error $\boldsymbol{\tau}$ for an unforced ($\mathbf{f} = 0$) system reads

$$\boldsymbol{\tau} = \mathscr{A}(\mathbf{y}_0, S_1, S_2, \Delta t) - \mathbf{y}_{ex}(\mathbf{y}_0, S_1, S_2, \Delta t), \tag{34}$$

where $\mathbf{y}_0$ defines the exact solution at time t_i. If $\boldsymbol{\tau} = O(\Delta t^{k+1})$ the algorithm is said to be of kth order [26, p. 132]. Expanding $\boldsymbol{\tau}$ in Taylor series about $\Delta t = 0$ up to the leading terms yields

$$\boldsymbol{\tau} = \begin{bmatrix} c_q(\mathbf{y}_0, S_1, S_2)\Delta t^{k_q} \\ c_p(\mathbf{y}_0, S_1, S_2)\Delta t^{k_q} \end{bmatrix}, \tag{35}$$

where the order of the algorithm is defined as $k = \min\{k_q - 1, k_p - 1\}$. The coefficients c_q and c_p are constant independent of Δt and are useful to point out the dependence of the local truncation error on the stiffness parameters for sufficiently small time steps.

In the linear case, Bonelli *et al.* [17] proved that the E-1C scheme endowed with $k_{max} = 1$, achieves the same accuracy order (third order) as the implicit parent TDG1 algorithm when

$$a = \tfrac{1}{3} - b. \tag{36}$$

In the non-linear case, c_q, $k_q c_p$ and k_p can be obtained using predictor (15) and one corrector (33). They are collected in Table 1; and it is clear that relation (36) entails third order accuracy also in the non-linear case. The use of equation (36) provides the τ values collected in Table 2. By perusing the results, it is evident that the E-2C scheme achieves the same accuracy as the implicit parent TDG1 algorithm, while the accuracy of the E-1C scheme depends on the free parameter b. Moreover, the E-2C scheme achieves third order accuracy without equation (36), and therefore, two free parameters a and b could be exploited. Nonetheless, we prefer to use relation (36) for the E-2C scheme also, as this relation is needed to achieve third order accuracy when an explicit damping treatment is considered [17]. Therefore, only one free parameter b is used to control the dissipative properties of the algorithms.

4.4. STABILITY

In the linear case, namely, $S_2 = 0$ in equation (42),

$$\mathscr{A} = \mathbf{A}\mathbf{y}_0 \tag{37}$$

in equation (23), where $\mathbf{A}$ is the so-called amplification matrix. This matrix is expressed at length in reference [17], and depends on the free parameter b and the non-dimensional frequency

$$\Omega = \sqrt{\frac{S_1}{M}}\,\Delta t \tag{38}$$

respectively. The stability properties of the E-1C and of the E-2C schemes are controlled by the eigenvalues $\lambda_{1,2}$ of $\mathbf{A}$ which assume the form

$$\lambda_{1,2} = e(\Omega, b) \pm \sqrt{h(\Omega, b)}. \tag{39}$$

The condition

$$h(\Omega, b) = 0 \tag{40}$$

corresponds to the bifurcation limit Ω_b, where $\lambda_{1,2}$ become real and distinct for $\Omega > \Omega_b$. Let ρ_b denote the spectral radius of $\mathbf{A}$ at the bifurcation limit Ω_b and Ω_{CR} the stability limit for which $\rho = 1$; Figures 2 and 3 plot the relations provided by condition (40) for the schemes E-1C and E-2C respectively. More specifically, these plots provide the value of b, which, employed in equations (15) and (36), permits a user-designed dissipation value ρ_b at the bifurcation limit to be achieved. For clarity, the above-mentioned figures also report the values of b, Ω_b and Ω_{CR} corresponding to $\rho_b = 0{\cdot}4$: $b = 0{\cdot}204$, $\Omega_b = 2{\cdot}022$ and $\Omega_{CR} = 2{\cdot}110$ for the E-1C scheme; and $b = 0{\cdot}404$, $\Omega_b = 2{\cdot}118$ and $\Omega_{CR} = 2{\cdot}318$ for the E-2C scheme. The expressions of b and Ω_b versus the design parameter ρ_b are expressed at length in reference [17].

In the non-linear case, the conservation or decay of the total energy (Hamiltonian) within a time step Δt is a sufficient condition for stability [27]. This energy criterion is expressed as

$$\frac{H_{i+1}}{H_i} \leqslant 1, \tag{41}$$

where $H_i = H(p_i, q_i)$ defines the Hamiltonian function of the system at time t_i. Hence, the energy ratio H_{i+1}/H_i is examined to provide a measure of the (energy) stability of the

TABLE 1

Accuracy properties of the explicit E-1C scheme

Algorithm	c_q	k_q	c_p	k_p
E-1C	$\frac{S_1^2(1+3q_0^2S_2)(1+q_0^2S_2)(-1+4b+8a)q_0}{24}$	4	$\frac{S_1^2(1+3q_0^2S_2)(1+q_0^2S_2)(-1+3b+3a)q_0}{6}$	3

TABLE 2

Accuracy properties both of the E schemes and of the implicit parent TDG1 scheme

Algorithm	c_q	k_q	c_p	k_p
E-1C	$-\frac{S_1^2(1+4q_0^2S_2+3q_0^4S_2^2)(-5+12b)q_0}{72}$	4	$\frac{S_1^2(-1+8(-2+3b)q_0^2S_2+(-19+24b)q_0^4S_2^2)p_0}{24}$	4
E-2C	$-\frac{S_1^2q_0(1+4q_0^2S_2+3q_0^4S_2^2)}{72}$	4	$-\frac{S_1^2(1+3q_0^4S_s^2)p_0}{72}$	4
TDG1	$-\frac{S_1^2q_0(1+4q_0^2S_2+3q_0^4S_2^2)}{72}$	4	$-\frac{S_1^2(1+3q_0^4S_s^2)p_0}{72}$	4

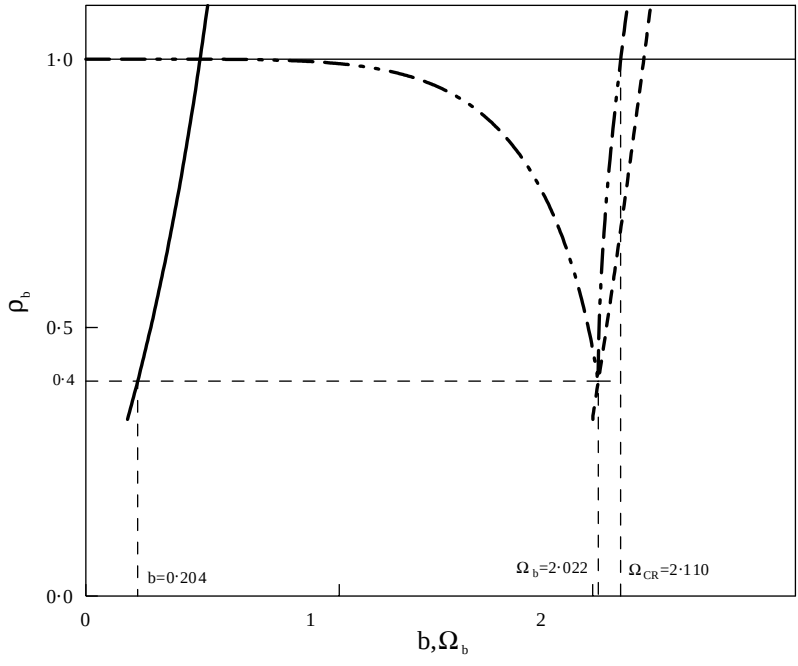

Figure 2. Relations among the spectral radius at the bifurcation limit ρ_b, the parameter b and the bifurcation limit Ω_b for the E-1C scheme (The scheme is unstable for $b < \frac{1}{6}$): ———, b; – – – – –, Ω_b; – – ·· – –, spectral radius for $\rho_b = 0{\cdot}4$.

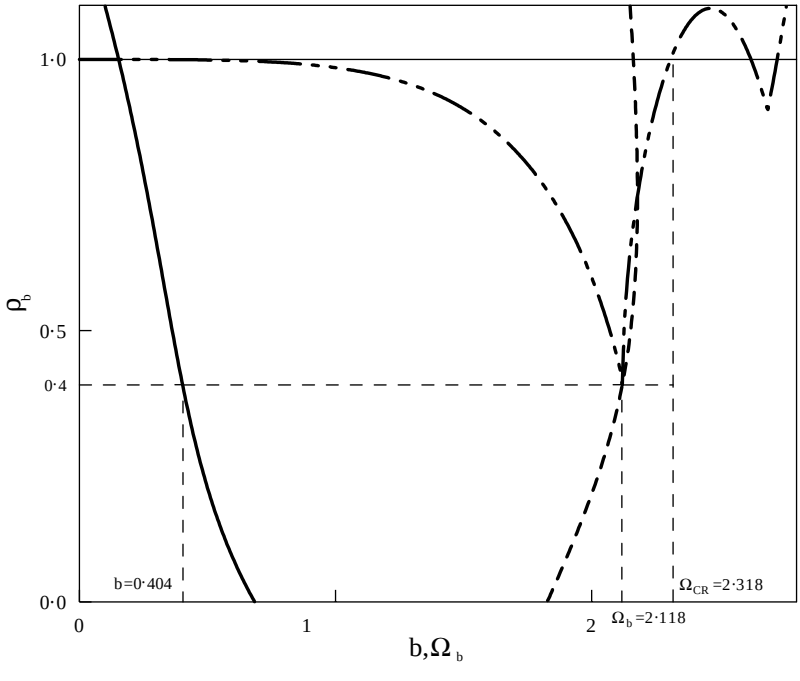

Figure 3. Relations among the spectral radius at the bifurcation limit ρ_b, the parameter b and the bifurcation limit Ω_b for the E-2C scheme; ———, b; – – – – –, Ω_b; – – ·· – –, spectral radius for $\rho_b = 0{\cdot}4$.

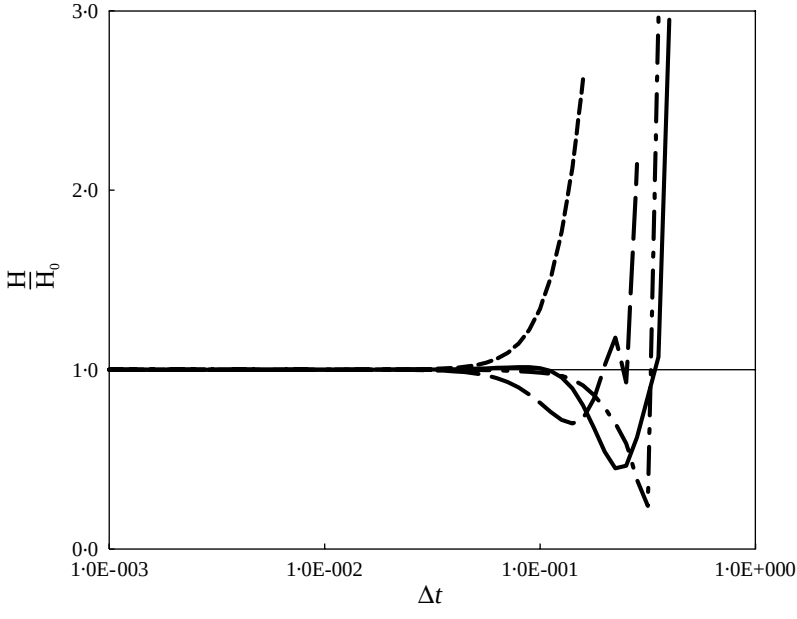

Figure 4. Hardening Duffing oscillator: evolution of the Hamiltonian ratio H/H_0 versus Δt; ———, E-1C $\rho_b = 0{\cdot}4$; — · — ·, E-2C $\rho_b = 0{\cdot}4$; —– —– —, CD; — — —, HCE-$\alpha\rho_b = 0{\cdot}4$.

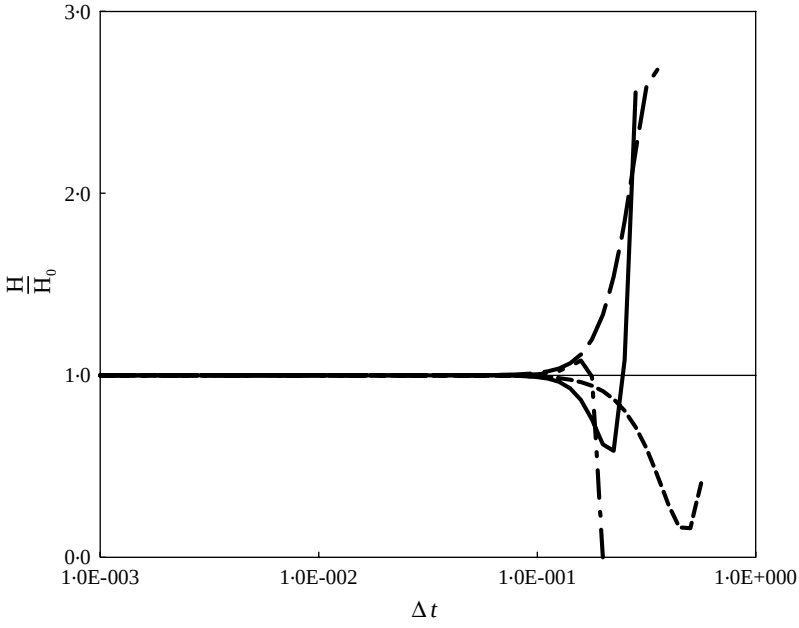

Figure 5. Softening Duffing oscillator: evolution of the Hamiltonian ratio H/H_0 versus Δt; ———, E-1C $\rho_b = 0{\cdot}4$; — · — ·, E-2C $\rho_b = 0{\cdot}4$; —– —– —, CD; — — —, HCE- $\alpha\rho_b = 0{\cdot}4$.

algorithms for non-linear problems. As no work is done by external and damping forces, a standard argument shows that $H(p, q)$ is a first integral of the problem, i.e., $H(p(t), q(t)) = H(p_0, q_0)$. A discrete energy-decay inequality has been proved for the implicit parent TDG1 algorithm applied to linear systems [11]. In the non-linear case, the energy

behaviour of the TDG method has been analyzed mainly through numerical experiments [19, 20].

With the unforced and undamped conservative Duffing oscillators at hand, both H and H_0 can be expressed through equation (48) which can be evaluated analytically by means of symbolic computation. Therefore, an energy stability analysis of the proposed E schemes can be performed. Assume $M = 1, S_1 = 100, p_0 = 0, q_0 = 1{\cdot}5, S_2 = 10$ and $q_0 = 1{\cdot}7, S_2 = -\frac{1}{3}$ to simulate strong hardening and softening systems respectively [25]. Moreover, choose the dissipation characteristics corresponding to the spectral radius $\rho_b = 0{\cdot}4$ (see Figures 2 and 3 respectively). The relevant Hamiltonian ratio H/H_0 versus Δt is depicted in Figures 4 and 5 for the hardening and softening systems respectively. For completeness, the E-1C and E-2C schemes are compared to the HCE-α method [9] with the same ρ_b value and to the CD scheme respectively. One can observe that the proposed E schemes achieve the energy conservation ($H/H_0 \to 1$) for $\Delta t \to 0$; moreover, they exhibit favourable stability and energy decay properties for large Δt values.

The energy behaviour of the E schemes has also been evaluated analytically for small Δt values, computing the leading term in the Taylor series expansion of $H/H_0 - 1$ at $\Delta t = 0$. Both c_H and k_H are collected in Table 3 as a function of Δt. One can infer that the E-2C scheme achieves the same result as the implicit parent TDG1 method. Moreover, the relevant value of c_H is negative for hardening systems, thus confirming its energy-decay properties in the non-linear case too. Conversely, c_H can reverse its sign for softening systems according to the values of the system parameters as well as of the initial conditions.

5. REPRESENTATIVE NUMERICAL SIMULATIONS

In this section, two representative numerical examples are introduced both to evaluate the performance of the E schemes and to warrant the analytical estimates in the non-linear case. To this end, initially s.d.o.f. Duffing oscillators are considered. They can model, for instance, the motion of a lumped mass attached to a taut string (hardening system) or reproduce the motion of a rigid pendulum (softening system). Moreover, such model problems have been exploited both to highlight the effect of high non-linearities on the stability properties of the trapezoidal rule [25] and to perform convergence studies [22, p. 306]. The second model problem deals with a two-degree-of-freedom system, namely, a stiff spring pendulum [3, 24]; it is characterized by the presence of a large and relatively slow circular motion and of a high-frequency axial motion, artefact of the finite element modelling. Since the two motions are coupled, the high-frequency dissipation of the spurious response is a desired feature. This example has also been selected to illustrate the loss of stability of some standard schemes in non-linear elastodynamics [3].

5.1. DUFFING OSCILLATORS

The unforced spring–mass Duffing oscillators are governed by the differential equation

$$M\ddot{q}(t) + S_1 q(t)(1 + S_2 q^2(t)) = 0, \tag{42}$$

where M is the mass, S_1 and S_2 are stiffness constants and $q(t)$ is the displacement from the equilibrium (zero internal force) position. In what follows, it is assumed that $M = 1, S_1 > 0$ and that the initial conditions are $q(0) = q_0$ and $\dot{q}(0) = p_0$. The differential equation (42) has been widely considered in dynamics, to reproduce both the motion of a hardening system ($S_2 > 0$, [8, 19]) and the motion of a softening system ($S_2 < 0$, [25]).

TABLE 3

Leading term of the Hamiltonian energy error both of the E schemes and of the implicit parent TDG1 scheme

Algorithm	c_H	k_H
E-1C	$-S_1^2\frac{((-5+12b)S_1(1+3q_0^2S_2)(q_0+q_0^3S_2)^2+p_0^2(3-24(-2+3b)q_0^2S_2+3(19-24b)q_0^4S_2^2))}{18(2p_0^2+2pq_0^2S_1+S_2q_0^4S_1}$	4
E-2C	$-S_1^2\frac{(S_1(1+3q_0^2S_2)(q_0+q_0^3S_2)^2+p_0^2(1+3q_0^4S_2^2))}{18(2p_0^2+2q_0^2S_1+S_2q_0^4S_1)}$	4
TDG1	$-S_1^2\frac{(S_1(1+3q_0^2S_2)(q_0+q_0^3S_2)^2+p_0^2(1+3q_0^4S_2^2))}{18(2p_0^2+2q_0^2S_1+S_2q_0^4S_1)}$	4

In view of both analysis and simulations, it is useful to provide the solution of equation (42). Since the non-linear term in the internal force is cubic in q, the solution can be easily expressed in terms of Jacobi elliptic functions [28, p. 92]. Let K(m) denote the complete elliptic integral of the first kind [29, p. 569] and consider $p_0 = 0$. In this case, the solution of hardening systems reads

$$q(t) = q_0 \,\mathrm{cn}(-\hat{\omega}t, m), \tag{43}$$

$$p(t) = q_0\hat{\omega}\,\mathrm{sn}(-\hat{\omega}t, m)\,\mathrm{dn}(-\hat{\omega}t, m), \tag{44}$$

where $\hat{\omega}^2 = S_1(1 + S_2q_0^2)$ and $m = S_2q_0^2/(2 + 2S_2q_0^2)$. The solution is periodic with period

$$T = \frac{4K(m)}{\hat{\omega}}. \tag{45}$$

The solution of softening systems is periodic if the initial displacement satisfies the inequality $|q_0| < 1/\sqrt{-S_2}$ [30, p. 108]. In this case, the solution can be written as

$$q(t) = q_0 \,\mathrm{sn}(\hat{\omega}t + K(m), m), \tag{46}$$

$$p(t) = q_0\hat{\omega}\mathrm{cn}(\hat{\omega}t + K(m), m)\,\mathrm{dn}(\hat{\omega}t + K(m), m), \tag{47}$$

where $\hat{\omega}^2 = S_1(2 + S_2q_0^2)/2$, $m = -S_2q_0^2/(2 + S_2q_0^2)$ and the period is still given by equation (45). For general initial conditions, the expressions become more complex. However, a Taylor series expansions of the solution about a given time $t = t_i$ can be obtained by

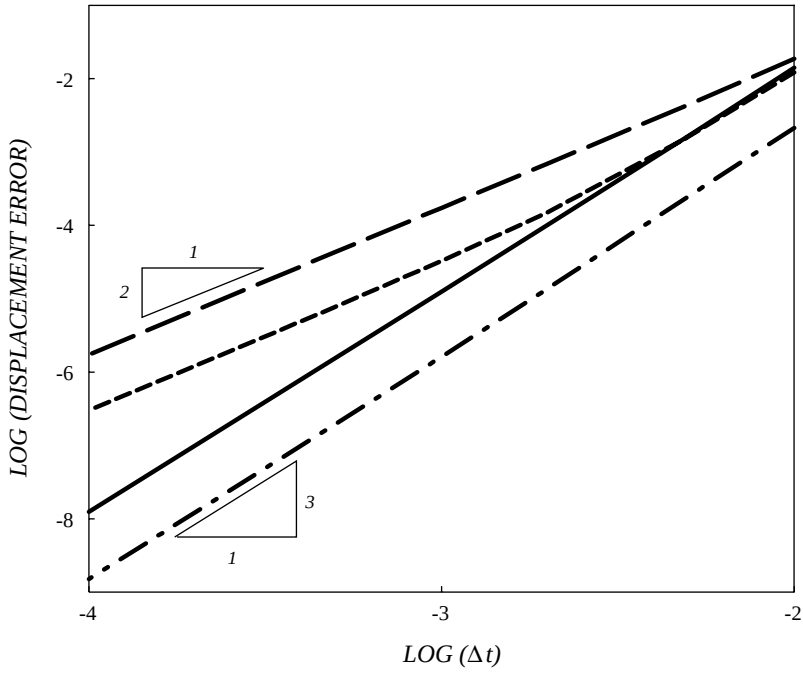

Figure 6. Hardening Duffing oscillator: convergence of displacement at $t = 0{\cdot}02$; ———, E-1C $\rho_b = 0{\cdot}4$; — · — ·, E-2C $\rho_b = 0{\cdot}4$; — — —, HCE-$\alpha\rho_b = 0{\cdot}4$; —– —– —, CD.

means of well-established methods [26, p. 41]. As the exact solutions are available, both the global displacement error $|q(t_i) - q_i|$ and the global momentum error $|p(t_i) - p_i|$ can be evaluated. Moreover, equation (42) describes an autonomous system, thus the Hamiltonian can be evaluated in the following form:

$$H(p(t), q(t)) = \tfrac{1}{2}\, p^2(t) + V(q(t)) = \tfrac{1}{2}\, p^2(t) + \tfrac{1}{2}\, S_1 q^2(t) + \tfrac{1}{2}\, S_1 S_2 q^4(t) = H(p_0, q_0), \quad (48)$$

where $V(q(t))$ defines the potential energy of the system.

Assume $S_1 = 100$; $S_2 = 10$; $q_0 = 1.5$ and $p_0 = 0{\cdot}0$ for the hardening oscillator, which entails a period $T = 0{\cdot}1515$; moreover, assume $S_1 = 100$; $S_2 = -\frac{1}{3}$; $q_0 = 1{\cdot}7$ and $p_0 = 0{\cdot}0$ for the softening oscillator. Since $|q_0| < 1/\sqrt{-S_2}$, the solution is periodic with period $T = 1{\cdot}5235$. The aforementioned parameters and initial conditions imply strong non-linear effects on the response [25].

With regard to the hardening oscillator, Figures 6 and 7 depict the global displacement error and the global momentum error, respectively, for the E schemes and the HCE-α scheme [9] with $\rho_b = 0{\cdot}4$, as well as for the CD method. The predictor–corrector E schemes exhibit third order accuracy, thus confirming the analytical estimates derived in section 4.3 and collected in Table 2; moreover, the errors relevant to the E schemes are smaller than those of traditional algorithms, thus confirming the favourable properties of the proposed methods. Figure 8 depicts the global displacement error relevant to both the E-2C and the HCE-α scheme for two values of the spectral radius at bifurcation: $\rho_b = 0{\cdot}4$ and $0{\cdot}6$, respectively. In the limit, the E-2C scheme accrues an error independent of the spectral radius ρ_b. Conversely, the HCE-α scheme exhibits an error which depends on ρ_b.

As far as the stability is concerned, the evolution of the Hamiltonian ratio H/H_0 is depicted in Figure 9, for the different algorithms at hand. Both the E-1C and the E-2C

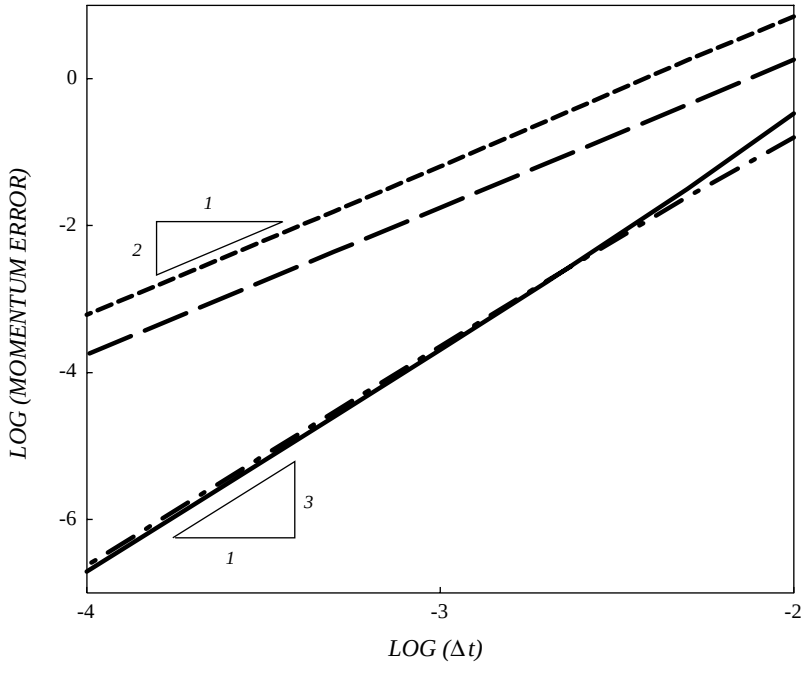

Figure 7. Hardening Duffing oscillator: convergence of momentum at $t = 0.02$; ———, E-1C $\rho_b = 0{\cdot}4$; — · — ·, E-2C $\rho_b = 0{\cdot}4$; — — —, HCE-$\alpha\rho_b = 0{\cdot}4$; —– —– —, CD.

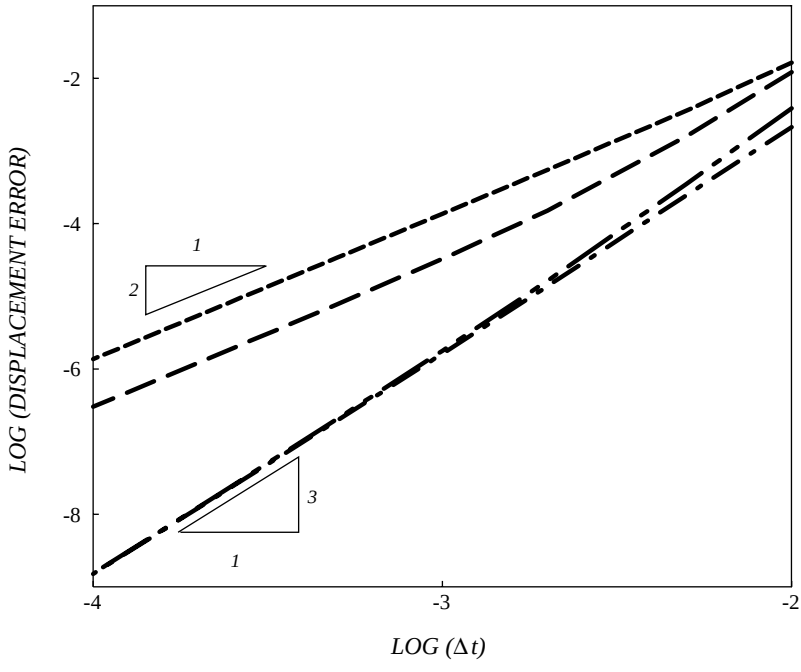

Figure 8. Hardening Duffing oscillator: convergence of displacement at $t = 0{\cdot}02$; — ·· —, E-2C $\rho_b = 0{\cdot}6$; — · — ·, E-2C $\rho_b = 0{\cdot}4$; – – – – –, HCE- $\alpha\rho_b = 0{\cdot}6$; — — —, HCE-$\alpha\rho_b = 0{\cdot}4$.

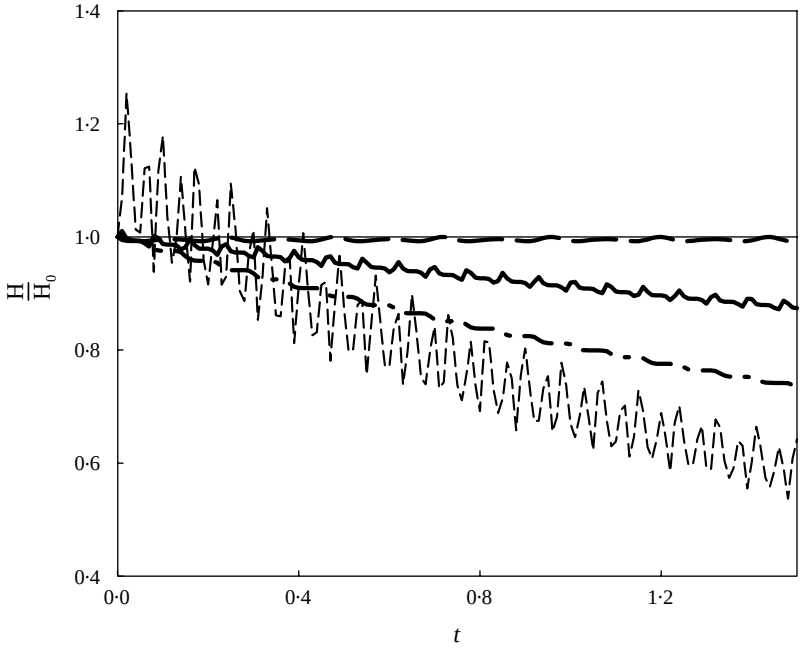

Figure 9. Hardening Duffing oscillator: evolution of the Hamiltonian ratio H/H_0 for $\Delta t = 0{\cdot}01$; ———, E-1C $\rho_b = 0{\cdot}4$; — ·— ·, E-2C $\rho_b = 0{\cdot}4$; —– —– —, CD; — — —, HCE-$\alpha\rho_b = 0{\cdot}4$.

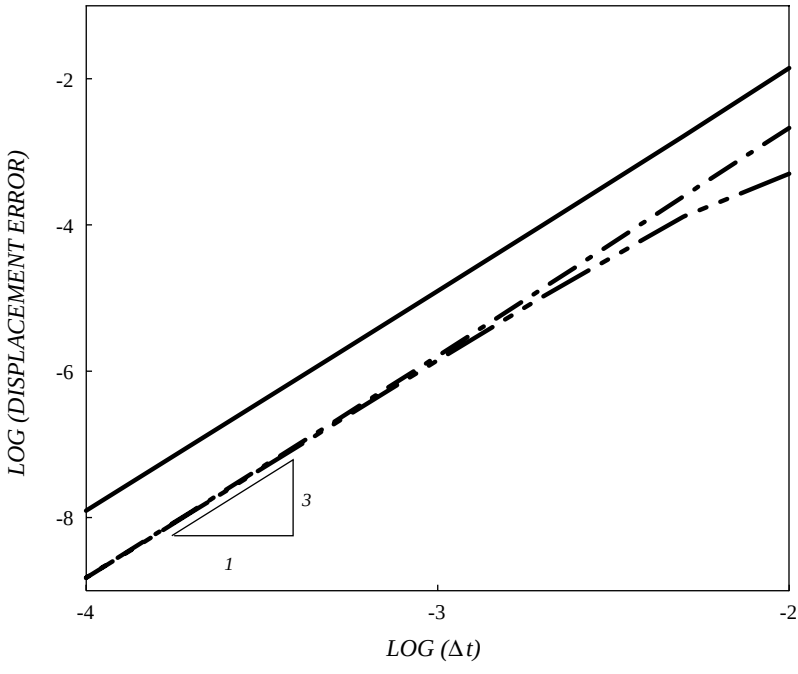

Figure 10. Hardening Duffing oscillator: convergence of coordinate at $t = 0{\cdot}02$; ———, E-1C $\rho_b = 0{\cdot}4$; — · —, E-2C $\rho_b = 0{\cdot}4$; — · · — ··, E-3C $\rho_b = 0{\cdot}4$.

scheme annihilate H/H_0, thus confirming the favourable energy-decaying properties of the E methods. The HCE-α method achieves better results in terms of global energy decay; however, the non-conservation of energy, a property already exhibited in the linear regime, as well as the approximate integration of the internal force in equation (42), entail oscillations which impair its overall performance. Conversely, the CD scheme exhibits its typical energy non-dissipative property; nonetheless, the energy is not exactly conserved either in the linear case.

The influence of the corrector number k_{max} both on the accuracy and on the energy stability of the E schemes can be inferred from Figures 10 and 11 respectively. The plots show clearly that the schemes with two (E-2C) and three (E-3C) corrector passes exhibit similar performance, pointing out that the choice $k_{max} = 2$ is adequate.

With regard to the softening oscillator, Figures 12 and 13 show the displacement error and the momentum error respectively. Again, the E schemes and the HCE-α method with $\rho_b = 0{\cdot}4$, as well as the CD scheme are considered. The relevant results confirm both the third order accuracy and the limited error achieved by the E schemes. The evolution of the Hamiltonian ratio H/H_0 is illustrated in Figure 14. Again, the favourable energy-dissipation properties of the E schemes and the oscillations of the HCE-α scheme are evident. Conversely, the CD scheme shows very limited dissipative properties.

5.2. STIFF SPRING PENDULUM

The stiff spring pendulum problem was analyzed on many occasions, see references [3, 24], among others; as a matter of fact, the axial response of the spring entails high-frequency components, artefact of modelling, which influence the rotational motion.

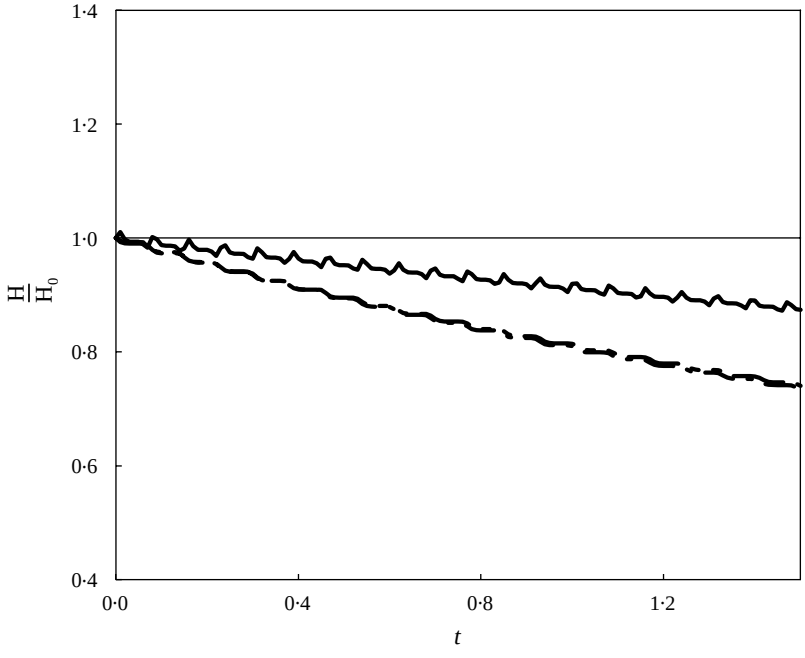

Figure 11. Hardening Duffing oscillator: evolution of the Hamiltonian ratio H/H_0 for $\Delta t = 0{\cdot}01$; ———, E-1C $\rho_b = 0{\cdot}4$; — · — ·, E-2C $\rho_b = 0{\cdot}4$; — · · — ··, E-3C $\rho_b = 0{\cdot}4$.

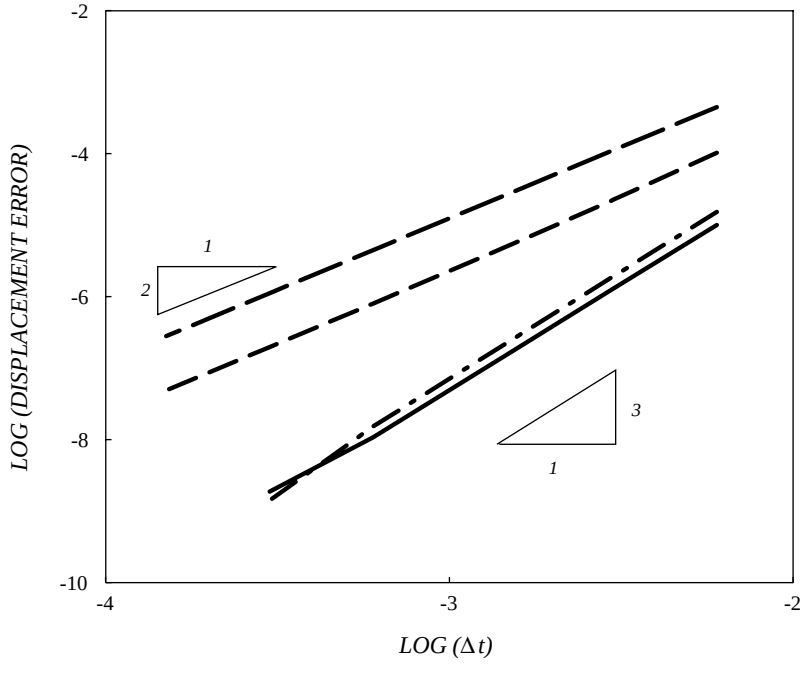

Figure 12. Softening Duffing oscillator: convergence of coordinate at time $t = 0{\cdot}3$; ———, E-1C $\rho_b = 0{\cdot}4$; — · — ·, E-2C $\rho_b = 0{\cdot}4$; — — —, HCE-$\alpha\rho_b = 0{\cdot}4$; —– —– —, CD.

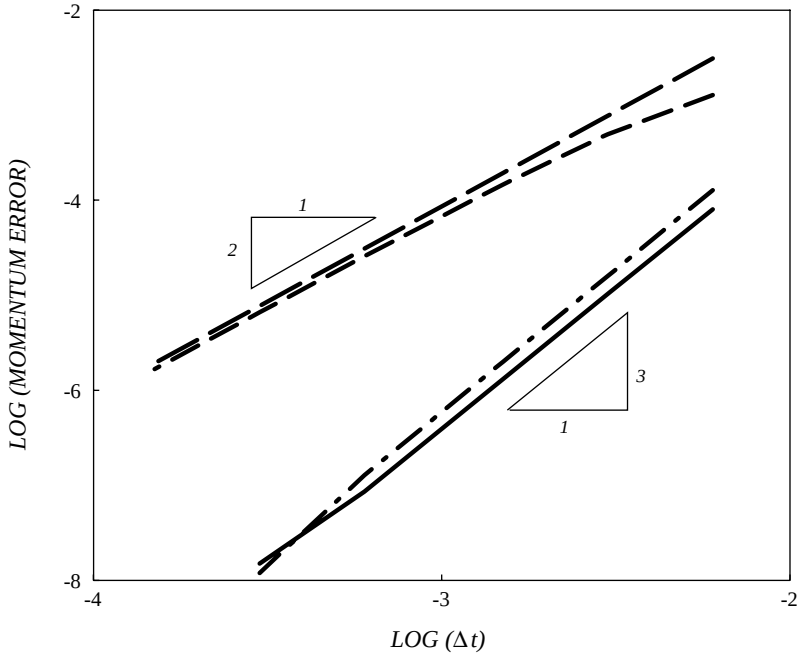

Figure 13. Softening Duffing oscillator: convergence of momentum at time $t = 0{\cdot}3$; ———, E-1C $\rho_b = 0{\cdot}4$; — · — ·, E-2C $\rho_b = 0{\cdot}4$; — — —, HCE-$\alpha\rho_b = 0{\cdot}4$; — – —, CD.

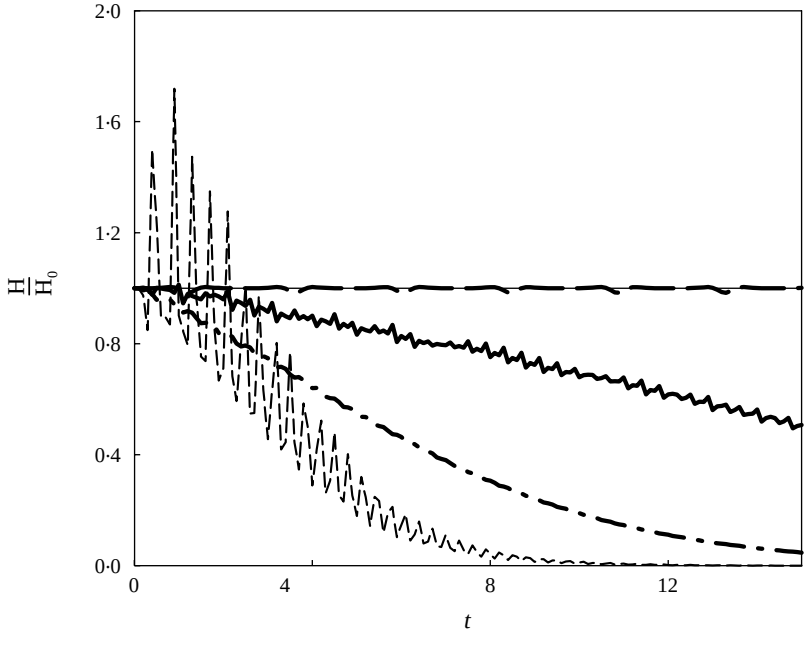

Figure 14. Softening Duffing oscillator: evolution of the Hamiltonian ratio H/H_0 for $\Delta t = 0{\cdot}1$; ———, E-1C $\rho_b = 0{\cdot}4$; — · — ·, E-2C $\rho_b = 0{\cdot}4$; — – —, CD; — — —, HCE-$\alpha\rho_b = 0{\cdot}4$.

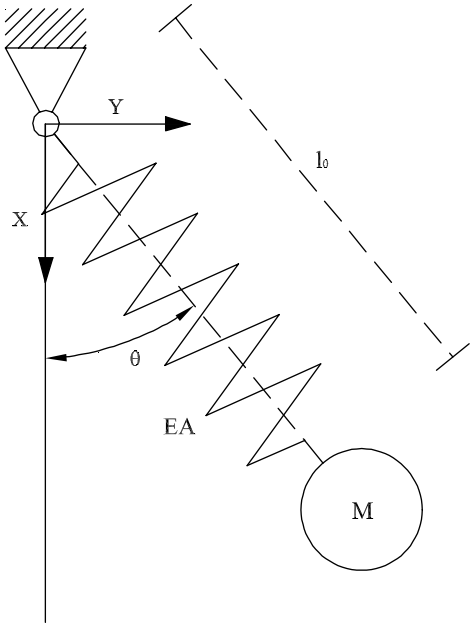

Figure 15. Stiff spring pendulum.

The stiff pendulum represents a variant of the rigid pendulum analyzed by several authors in the past (see reference [2, p. 452], and references therein). Hereinafter, the approach suggested in reference [3] is followed. Therefore, the stiff spring pendulum is discretized with a truss element formulated in the total Lagrangian description with the assumption of a Saint Venant Kirchhoff material model. In fixed Cartesian co-ordinates X and Y, see Figure 15, the stiff spring pendulum with no gravity can be expressed as

$$\begin{aligned} \dot{p}_x + \frac{EA_0}{l_0}\varepsilon_G q_x = 0, \\ \dot{p}_y + \frac{EA_0}{l_0}\varepsilon_G q_y = 0, \end{aligned} \tag{49}$$

where A_0 and l_0 are the cross-section and the length in the reference configuration, respectively, E is Young's modulus and ε_G is Green strain defined as

$$\varepsilon_G = \frac{\sqrt{q_x^2 + q_y^2} - l_0}{l_0} + \frac{1}{2}\left(\frac{\sqrt{q_x^2 + q_y^2} - l_0}{l_0}\right)^2. \tag{50}$$

The pendulum conserves the total mechanical energy, or Hamiltonian, which has the form

$$H(p, q) = \frac{1}{2M}(p_x^2 + p_y^2) + \frac{1}{2} EA_0 l_0 \varepsilon_G^2, \tag{51}$$

where $M = \frac{1}{2}\rho_0 A_0 l_0$ and ρ_0 is the density in the reference configuration. It is endowed with $l_0 = 3{\cdot}0443$ m, $\rho_0 A_0 = 6{\cdot}57$ kg/m, $EA_0 = 1{\cdot}4137 \times 10^6$ N and it is powered by an initial tangential velocity $\dot{u}_0 = 7{\cdot}72$ m/s. Hence $\mathbf{q}_0 = (l_0 \text{ m}, 0 \text{ m})^{\mathrm{T}}$ and $\mathbf{p}_0 = (0 \text{ kg (m/s)}, 10 \times 7{\cdot}72 \text{ kg (m/s)})^{\mathrm{T}}$. As no initial radial acceleration is applied, the truss is loaded by

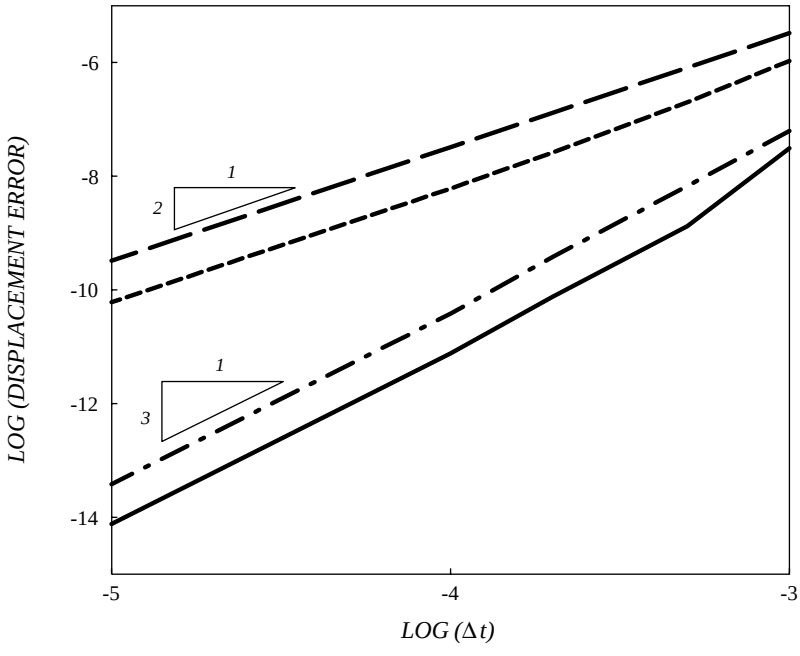

Figure 16. Stiff spring pendulum: convergence of q_x at $t = 0{\cdot}02$ s; ———, E-1C $\rho_b = 0{\cdot}4$; — · — ·, E-2C $\rho_b = 0{\cdot}4$; — – —, CD; — — —, HCE-$\alpha\rho_b = 0{\cdot}4$.

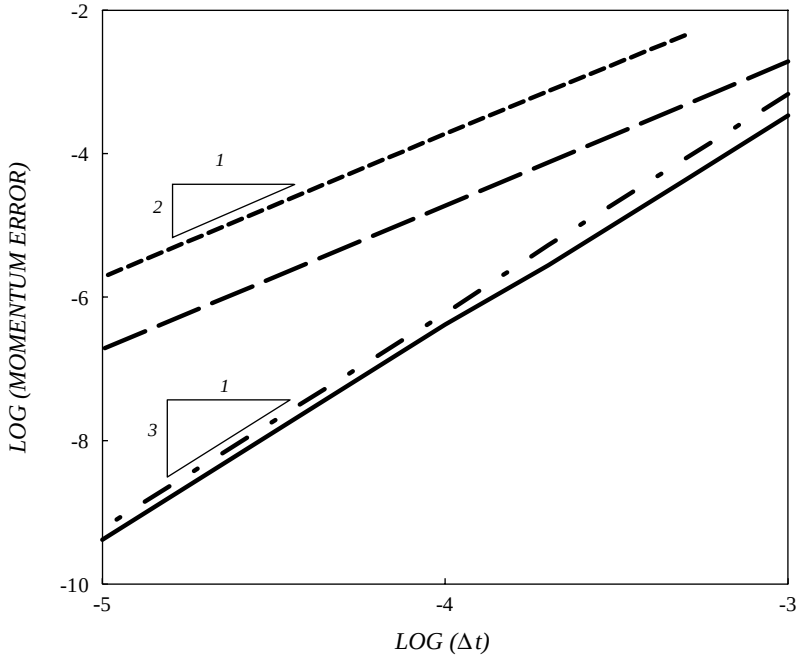

Figure 17. Stiff spring pendulum: convergence of p_x at $t = 0.02$ s; ———, E-1C $\rho_b = 0{\cdot}4$; — · — ·, E-2C $\rho_b = 0{\cdot}4$; — – —, CD; — — —, HCE-$\alpha\rho_b = 0{\cdot}4$.

the centrifugal force which stimulates the high-frequency axial vibration. Moreover, the axial and rotational motion are coupled by the Coriolis force. The uncoupled axial vibration period is $T_{ax} = 0{\cdot}029$ s while the rotation period amounts to $T_{rot} \cong 2{\cdot}48$ s

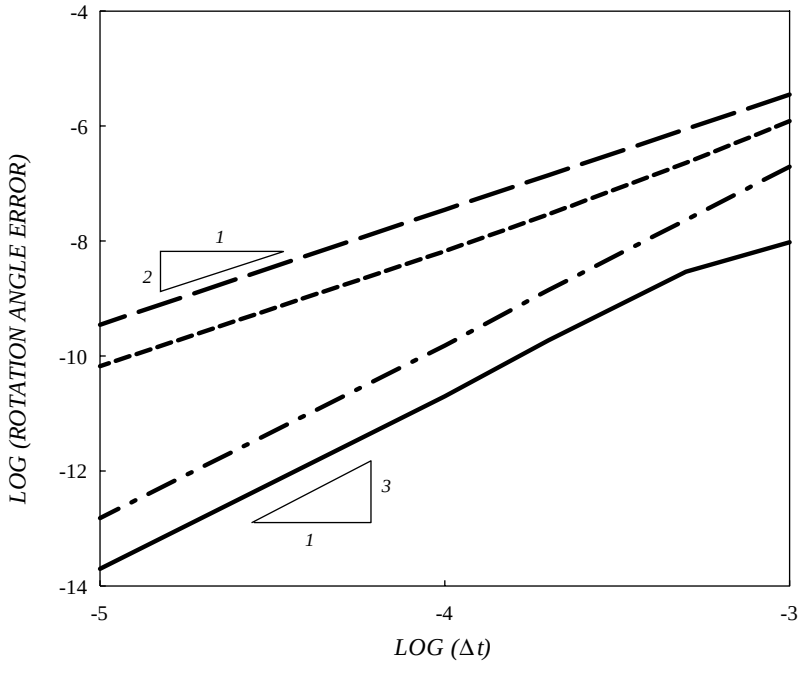

Figure 18. Stiff spring pendulum: convergence of the rotation angle at $t = 0{\cdot}02$ s; ———, E-1C $\rho_b = 0{\cdot}4$; — · — ·, E-2C $\rho_b = 0{\cdot}4$; — – —, CD; — — — , HCE-$\alpha\rho_b = 0{\cdot}4$.

assuming rigid-body motion. As a result, this system results axially two orders of magnitude stiffer than the one considered in reference [3]; therefore, the E schemes must damp out the undesirable high-frequency axial response without introducing excessive algorithmic damping in the low-frequency rotational response. The exact solution is not available and therefore, the reference solution is derived from the CD method employing a very small time step. Moreover, the exact integration of equations (9_1) and (9_2) is not available, and thus the E scheme exploits a three-point Gauss–Legendre quadrature. Besides the primary unknown vector $\mathbf{q} = (q_x, q_y)^{\mathrm{T}}$, the circular co-ordinates θ and $\Delta l = \sqrt{q_x^2 + q_y^2} - l_0$ have also been traced.

Figures 16–18 show the co-ordinate q_x, the momentum p_x, and the rotation angle θ errors, respectively, at time $t = 0{\cdot}02$ s. Results are relevant to the E and the HCE-α schemes with $\rho_b = 0{\cdot}4$ as well as to the CD method. Again, the results confirm the good accuracy properties of the E schemes as well as the analytical estimates presented in section 0·3. Note that the low error of the E-1C scheme depends on the initial conditions. The subsequent simulations assume a time step $\Delta t = 0{\cdot}009$s close to the stability limit of the CD method. Such conditions are chosen in order to integrate properly the rotational motion and annihilate the axial motion. However, they render the HCE-α method unstable. The time evolution of the Hamiltonian ratio H/H_0 is reported in Figure 19, and it can be observed that few steps are sufficient to the E schemes, to annihilate spurious oscillations caused by axial motion. Conversely, the CD method exhibits spurious energy oscillation due to high axial frequencies. The effects of such spurious frequencies on the performance of the CD method are evident in Figure 20, where the evolution of the axial displacement Δl is reported. The limited dissipation properties of the CD method and the favourable properties of the E schemes are evident. The time history of the rotation angle error relevant

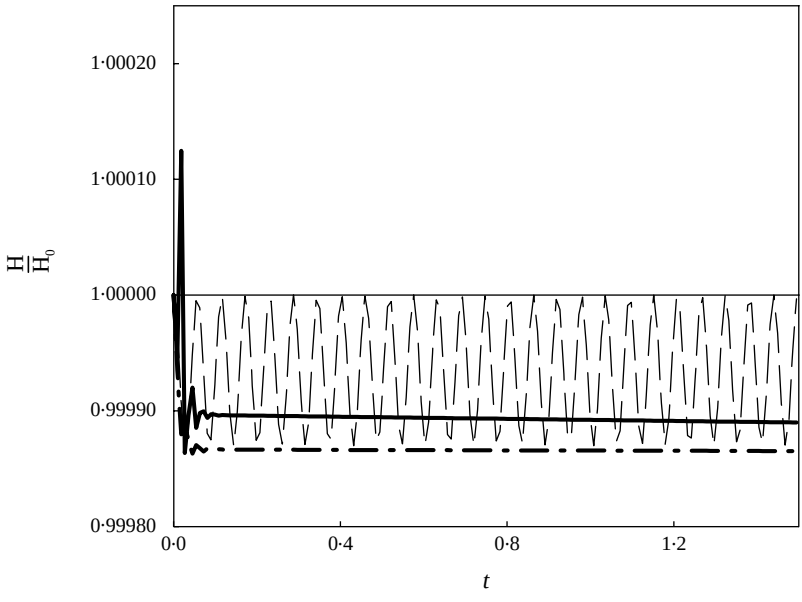

Figure 19. Stiff spring pendulum: evolution of the Hamiltonian ratio H/H_0 for $\Delta t = 0{\cdot}009$ s; ———, E-1C $\rho_b = 0{\cdot}4$; — · — ·, E-2C $\rho_b = 0{\cdot}4$; — – —, CD.

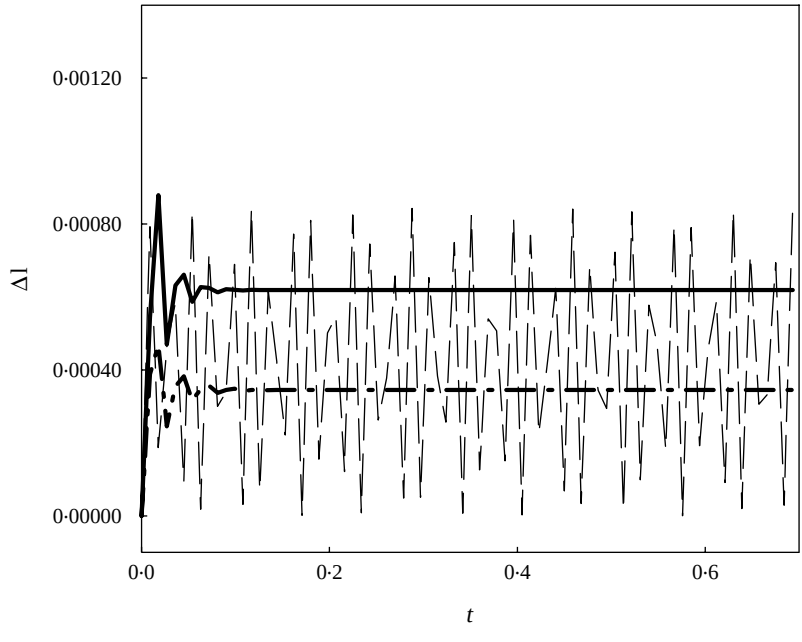

Figure 20. Stiff spring pendulum: evolution of the axial displacement for $\Delta t = 0{\cdot}009$ s; ———, E-1C $\rho_b = 0{\cdot}4$; — · — ·, E-2C $\rho_b = 0{\cdot}4$; — – —, CD.

to the previous simulation is highlighted in Figure 21. The good accuracy properties of the E-2C scheme with respect to those of the CD method are evident.

Finally, the Hamiltonian ratio H/H_0 is plotted in Figure 22 as a function of Δt at the second time step. This step was chosen because it can be proved that the initial conditions

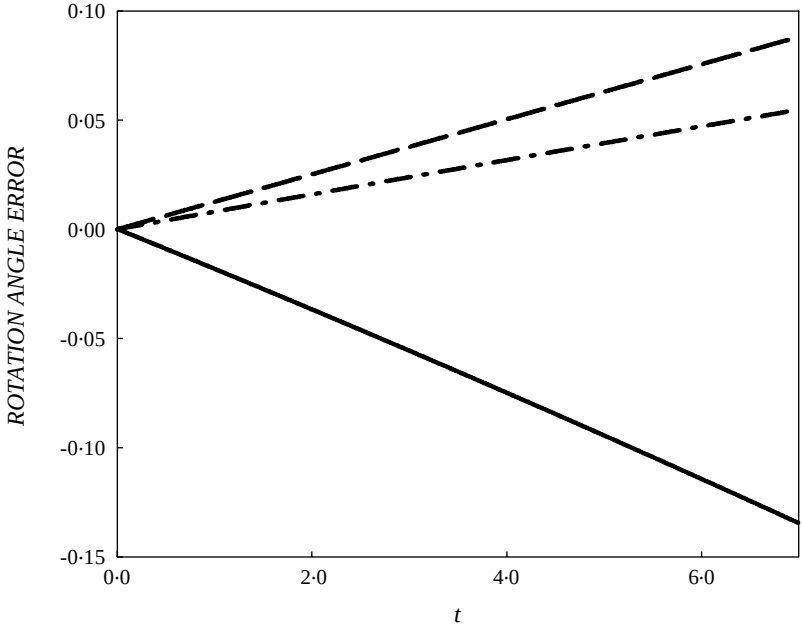

Figure 21. Stiff spring pendulum: evolution of the rotation angle error for $\Delta t = 0.009$ s; ———, E-1C $\rho_b = 0{\cdot}4$; — · — ·, E-2C $\rho_b = 0{\cdot}4$; — – —, CD.

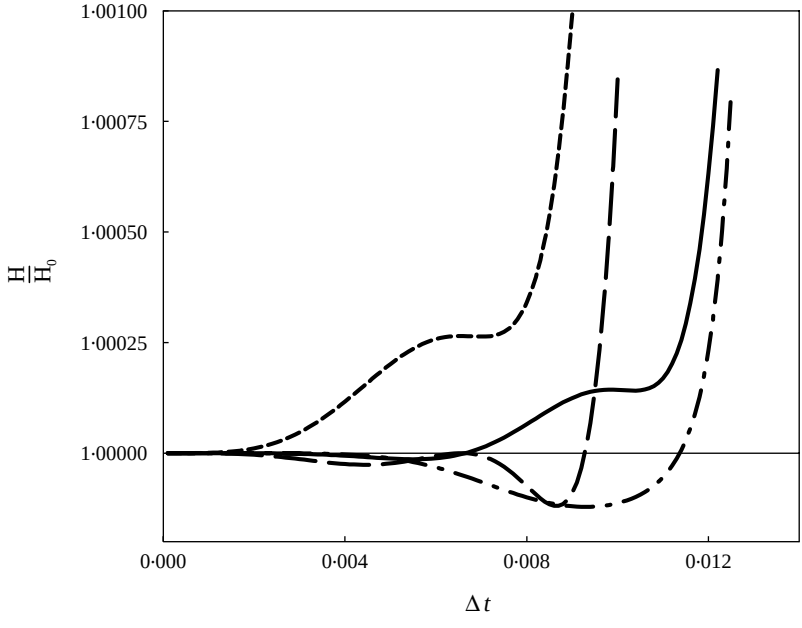

Figure 22. Stiff spring pendulum: H/H_0 versus Δt; ———, E-1C $\rho_b = 0{\cdot}4$; — · — ·, E-2C $\rho_b = 0{\cdot}4$; — – —, CD; — — —, HCE-α $\rho_b = 0{\cdot}4$.

considered, allow the E-1C and the E-2C schemes to be fifth and seventh order accurate, respectively, at the first time step. As a result, the plots of Figure 22 are relevant to the second time step, which implies third order accuracy for both schemes. Again the favourable

performance of the E methods, especially that of the E-2C scheme, is evident. In fact, the E-2C scheme exhibits a higher stability limit than those of the other schemes as well as favourable dissipation properties.

6. CONCLUDING REMARKS

In this work, we have studied predictor–multicorrector time discontinuous Galerkin (TDG) methods applied to non-linear problems. More specifically, the explicit time-stepping schemes developed in reference [17] and resulting in one- and two-pass corrector procedures have been analyzed through conservative Duffing oscillators, for which closed-form solutions are available, showing that both third order accuracy and energy-decaying properties can be retained also in the context of relatively simple non-linear test problems. The proposed schemes have performed satisfactorily in numerical simulations of conservative Duffing oscillators and the results appear to be in a good agreement with analytical estimates. Moreover, the predictor–multicorrector schemes have been applied to a stiff spring pendulum showing that such time-stepping methods are particularly attractive for time integration of finite element semidiscrete problems, where advantage can be taken of the high-frequency dissipation properties. In fact, simulations have indicated that the influence of the high-frequency internal axial motion on the global circular motion can be limited. Both analysis and numerical simulation highlight the favourable accuracy and dissipative properties of the explicit TDG schemes when compared to those of standard finite difference-based methods, and render the proposed predictor–multicorrector schemes competitive for medium-term high-quality analyses.

ACKNOWLEDGMENTS

The financial support from the Italian Ministry for Universities and Scientific and Technological Research (MURST) is acknowledged. However, opinions expressed in this paper are those of the writers, and do not necessarily reflect the views of the sponsoring agency.

REFERENCES

1. T. J. R. HUGHES 1987 *The Finite Element Method, Linear Static and Dynamic Finite Element Analysis*. Englewood Cliffs, NJ: Prentice-Hall.
2. M. A. CRISFIELD 1994 *Non-linear Finite Element Analysis of Solids and Structures Volume* 1: *Essentials*. New York: John Wiley & Sons.
3. D. KUHL and A. CRISFIELD 1999 *International Journal for Numerical Methods in Engineering* **45**, 569–600. Energy conserving and decaying alghorithms in non-linear structural dynamics.
4. J. CHUNG and J. M. LEE 1994 *International Journal for Numerical Methods in Engineering* **37**, 3961–3976. A new family of explicit time integration methods for linear and non-linear structural dynamics.
5. R. W. MACEK and B. H. AUBERT 1995 *Earthquake Engineering and Structural Dynamics* **24**, 1315–1331. A mass penalty technique to control the critical time increment in explicit dynamic finite element analyses.
6. Z. WANXIE, X. ZHUANG and J. ZHU 1998 *Applied Mathematics and Computation* **89**, 295–312. A self-adaptive time integration algorithm for solving partial differential equations.
7. C. HOFF and R. L. TAYLOR 1990 *International Journal for Numerical Methods in Engineering* **29**, 275–290. Higher derivative explicit one step methods for non-linear dynamic problems. Part I: design and theory.

8. C. HOFF and R. L. TAYLOR 1990 *International Journal for Numerical Methods in Engineering* **29**, 291–301. Higher derivative explicit one step methods for non-linear dynamic problems. Part II: practical calculations and comparison with other higher order methods.
9. G. M. HULBERT and J. CHUNG 1996 *Computer Methods in Applied Mechanics and Engineering* **137**, 175–188. Explicit time integration algorithms for structural dynamics with optimal numerical dissipation.
10. G. M. HULBERT 1994 *Computer Methods in Applied Mechanics and Engineering* **113**, 1–9. A unified set of single step asymptotic annihilation algorithms for structural dynamics.
11. M. BORRI and C. BOTTASSO 1993 *Computational Mechanics* **13**, 133–142. A general framework for interpreting time finite element formulations.
12. M. CANNAROZZI and M. MANCUSO 1995 *Computer Methods in Applied Mechanics and Engineering* **127**, 241–257. Formulation and analysis of variational methods for time integration of linear elastodynamics.
13. T. C. FUNG and A. Y. T. LEUNG 1996 *Journal of Vibration and Control* **2**, 193–217. On the accuracy of discontinuous Galerkin methods in the time domains.
14. X. D. LI and N. E. WIBERG 1996 *International Journal for Numerical Methods in Engineering* **39**, 2131–2152. Structural dynamics analysis by a time-discontinuous Galerkin finite element method.
15. N. E. WIEBERG and X. D. LI 1997 in *Proceedings of COMPLAS V*: *Computational Plasticity*, *Fundamentals and Applications*, *Barcellona*, *CIMNE*) 224–237, (D. R. J. Owen, E. Onate and E. Hinton, editors), Implicit and explicit discontinuous Galerkin finite element procedures for linear and nonlinear structural dynamic analysis.
16. N. E. WIBERG and X. D. LI 1999 *International Journal for Numerical Methods in Engineering* **46**, 1781–1802. Adaptive finite element procedures for linear and non-linear dynamics.
17. A. BONELLI, O. S. BURSI and M. MANCUSO 2001 *Journal of Sound and Vibration* **246**, 625–652. Explicit predictor–multicorrector time discontinuous Galerkin methods for linear dynamics.
18. J. ARGYRIS and H-P. MLEJNEK 1991 *Dynamics of Structures*. Amsterdam: North-Holland.
19. P. Z. BAR-YOSEPH, D. FISCHER and O. GOTTLIEB 1996 *Computational Mechanics* **18**, 302–313. Spectral element methods for nonlinear temporal dynamical system.
20. P. Z. BAR-YOSEPH, D. FISCHER and O. GOTTLIEB 1996 *Computational Mechanics* **19**, 136–151. Spectral element methods for nonlinear spatio-temporal dynamics of an Euler–Bernoulli beam.
21. Y. M. XIE and G. P. STEVEN 1994 *Communication in Applied Numerical Methods* **10**, 393–401. Instability, chaos, and growth and decay of energy time-stepping schemes for nonlinear dynamic equations.
22. W. L. WOOD 1990 *Practical Time-Stepping Schemes*. Oxford: Clarendon Press.
23. E. HAIRER and G. WANNER 1991 *Solving Ordinary Differential Equations II*. Berlin: Springer-Verlag.
24. J. YEN, L. PETZOLD, and S. RAHA 1998 *Computer Methods in Applied Mechanics and Engineering* **158**, 341–355. A time integration algorithm for flexible mechanism dynamics the dae alpha-method.
25. W. L. WOOD and M. E. ODUOR 1988 *Communications in Applied Numerical Methods* **4**, 205–212. Stability properties of some algorithms for the solution of nonlinear dynamics vibration equations.
26. E. HAIRER, S. P. NORSETT and G. WANNER 1987 *Solving Ordinary Differential Equations I. Nonstiff Problems*. Berlin: Springer-Verlag.
27. T. BELYTSCHKO and D. F. SCHOEBERLE 1975 *Journal of Applied Mechanics* **42**, 865–869. On the unconditional stability of an implicit algorithm for nonlinear structural dynamics.
28. F. DINCA and C. TEODOSIU 1973 *Nonlinear and Random Vibration*. London: Academic Press.
29. M. ABRAMOWITZ and I. A. STEGUN 1964 *Handbook of Mathematical Functions*. Applications of Mathematics, Series, Vol. 55. Washington, DC: National Bureau of Standards.
30. M. FARKAS 1994 *Periodic Motions*. Berlin: Springer-Verlag.